Product Development Team
for
Advanced Weather Radar Techniques
Quarterly Report – 1st Quarter FY 04

04.6.2 Polarization and Frequency Diversity

Algorithms based on polarimetry will meet the aviation needs for information about the volumetric extent of hail, freezing rain, snow, and icing conditions, as well as non-hydrometeor scatterers. The biggest potential payoff is enhanced data quality. For all practical purposes, polarimetric techniques will eliminate problems associated with sea-clutter, ground clutter, AP, and biological scatterers.

a) Current Efforts

(NSSL):

Radar data quality improvement. Calibration issues of dual-polarization measurments.

Report contained in Appendix 1.

(NCAR):

Task 04.6.2.7 Investigation of winter storm cases.

Computer procedures for processing the 2-D video disdrometer measurements were completed during the quarter. The procedure for determining snow density was tested on a rain event (Fig. 1). The water mass is computed from three GEONOR gauges, and the precipitation volume is determined by summing the incremental volumes of individual raindrops detected with the disdrometer. The computed precipitation density averages about 1.05 g cm^{-3}, a small overestimate. The source of the bias has not been determined but should not prevent usable estimates of snow density.

The method is applied to a snow event in Fig. 2. Snow densities of 0.05 to 0.25 g cm^{-3} are indicated. The high densities in this case are due to the relatively warm temperatures (0.5 to 1^{o}C) and the fact that melting has begun. Inspection reveals little correlation between snow density and other parameters, e.g., precipitation rate. As found with other events, visibility is only partly correlated with precipitation rate, suggesting that a multi-sensor approach is needed for its prediction.

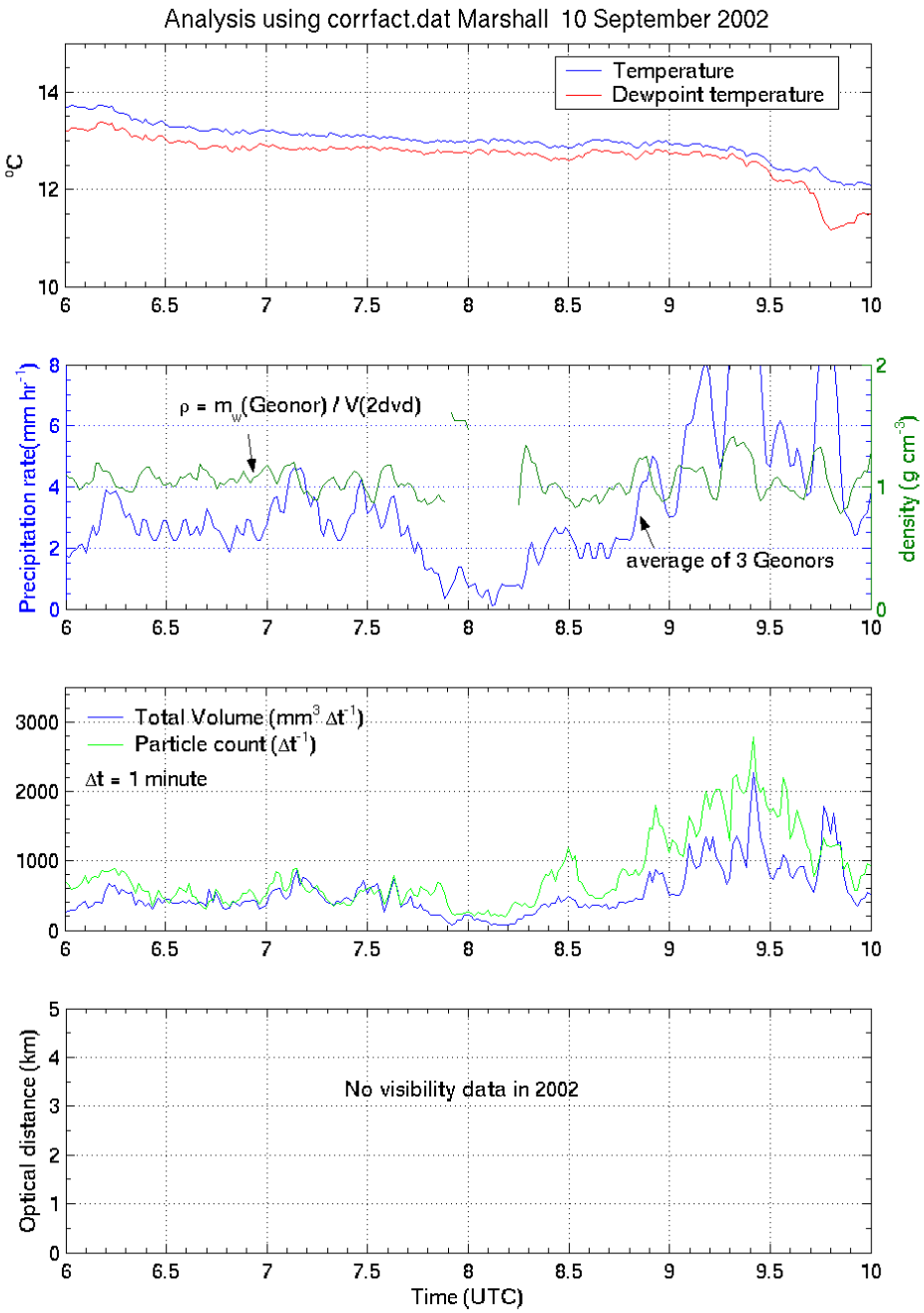

Figure 1. Rain event of 10 Sep 2002. Upper panel shows dry-bulb and dew-point temperatures. Second panel presents rain rate and precipitation density. Third panel gives precipitation volume and particle (drop) rate per minute as measured by the disdrometer.

c) Problems/Issues

None.

d) Interface with other Organizations

None.

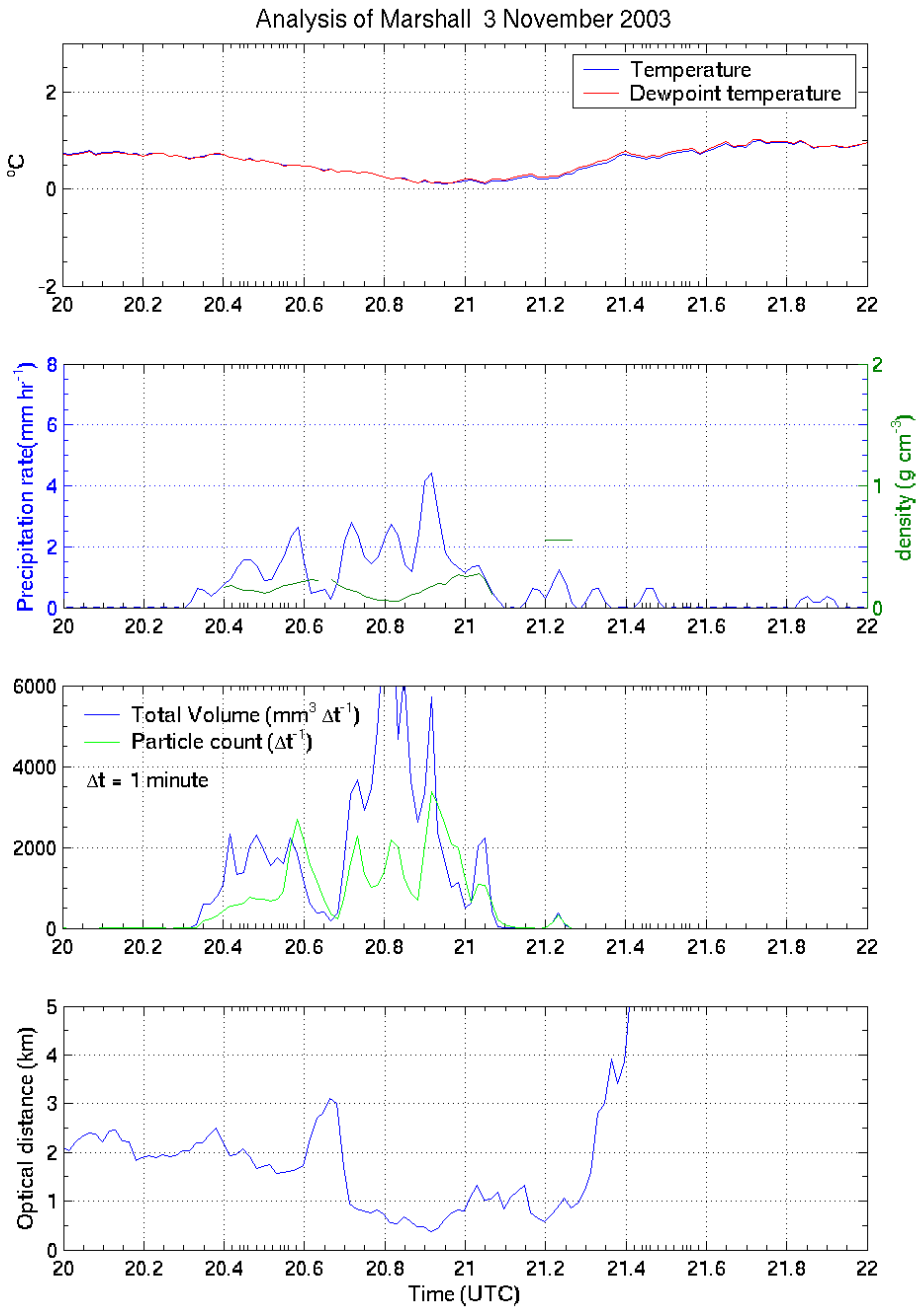

Figure 2. As in Fig. 1, except for snow event of 3 Nov 2003. Fourth panel shows optical distance (visibility).

e) Activity Schedule Changes

None.

04.6.3 Circulations

Particularly violent or long-lived storms tend to possess certain notable qualities, including, for example, mesocyclones. The current WSR-88D algorithms have a very high false alarm rate. Controllers find such high false alarm rates unacceptable. To mitigate this problem, new more robust and reliable circulation detection algorithms will be developed. Algorithms that use circulations to diagnose storm severity or estimate storm longevity will be considerably improved by this work.

a) Current Efforts

No activity in Q1.

b) Planned Efforts

Activity expected to commence in Q2

c) Problems/Issues

None.

d) Interface with other Organizations

None.

e) Activity Schedule Changes

None.

04.6.4 Technical Facilitation

Technical facilitation supports the NEPDT algorithm development. There is currently no standard vehicle outside of NSSL for algorithm development support. The interface being developed at the NSSL, the WDSS-II, provides a way to develop, validate, verify and demonstrate the NEXRAD algorithms developed within this PDT. Additionally, WDSS-II provides a route into the Open Radar Product Generation (ORPG) system. WDSS-II will support and incorporate the MITRE Common Operations Development Environment (CODE). WDSS-II is an important ingredient for the overall success of the NEPDT because, in consonance with CODE, coding and testing standards at the application prototype level are enforced. Transfer of single-radar algorithms to the ROC will be straightforward, as anything within WDSS-II must also conform to CODE standards. Overall, NEPDT efforts will inevitably enhance the algorithms that have been accepted or will be implemented by the ROC as part of the WSR 88D system.

a) Current Efforts

Full report is attached as Appendix 2.

b) Planned Efforts

Continue work on developing 3-level iso-surfacing of radar data for 3D visualization.

c) Problems/Issues

None.

d) Interface with other Organizations

None.

e) Activity Schedule Changes

None.

04.6.12 Product Implementation

Product implementation is a the process by which implementation paths are explored and defined within the aviation community systems that are best for NEPDT products. This process includes collaboration with other PDTs to help define the nature of WSR-88D they need. Technical facilitation also includes the low-level process of defining technical details (formats, data set file structures, etc.) of the products developed NEPDT.

a) Current Efforts

Extensive meetings held with NCAR, ETL and MIT LL concerning the reorganization of the NEPDT into the AWRT. Meetings also held with FSL to make 3-D mosaic data available to FSL.

Also provided significant guidance to Howard Eichenbaum of MCR for a cost/benefit analysis of AWRT activities and development.

b) Planned Efforts

Continue process for completing the AWRT reoganization.

c) Problems/Issues

None.

d) Interface with other Organizations

None.

e) Activity Schedule Changes

None

04.6.13 TDWR/NEXRAD Techniques Development.

Data from the TDWR has significantly higher spatial and temporal resolution than data from the WSR-88D. In addition, the TDWR can fill in low-altitude coverage unavailable to the WSR-88D due to range limitations. Because of different scanning strategies and missions, algorithms for the two radars are not usually mutually compatible. Hence the development of techniques similar to those for the WSR-88D, to accommodate the TDWR.

a) Current Efforts

The activities for this quarter include archiving the OKC TDWR and KTLX WSR-88D radar data for a winter storm case which occurred in early November. Twelve additional cases with OKC TDWR and KTLX WSR-88D data, ranging from winter storms, spring-summer time convective systems, and tornadoes, are compiled from last year's archiving. Analysis of the TDWR and co-located WSR-88D radar data for these cases are undergoing.

b) Planned Efforts

Analyses and intercomparisons of TDWR radar echoes and WSR-88D radar echoes will continue.

c) Problems/Issues

None.

d) Interface with other Organizations

None.

04.6.14 Multi-radar Composites

The area for which any arbitrary ARTCC has responsibility likely encompasses the coverage area of several WSR-88D installations. Neither the ROC nor the NWS has plans to treat the various WSR-88D installations as a single network, so there are no existing algorithms that use data from more than one radar. This is a serious limitation, because treating each radar separately leads to ambiguities when the radar data overlap. Currently, the users must independently mitigate these ambiguities, which requires significant knowledge about meteorological radar data and the nature of the algorithms that are run on these data. Aviation users generally do not possess this knowledge, so for the WSR-88Ds to be treated as a network, algorithms and techniques aimed specifically at multiple radar composites must be developed.

a) Current Efforts

04.6.14.1 3-D mosaic survey to the AWRP Product Development Teams

A survey was prepared and disseminated to all PDTs to determine the extent at which they use products from the 3D mosaic. The Convective Weather PDT and the Winter Weather Research PDT have used the CIWS domain 3D reflectivity mosaic in their model simulations in the last year. During this quarter, other PDTs were surveyed on the usage and future enhancements of the 3D mosaic. The MDEPDT showed interest of using the 3D reflectivity mosaic over a CONUS domain for model data assimilations and for verifications. The MDEPDT also provided useful insights on the enhancements of the 3D mosaic. Below is a summary of the survey results and proposed strategies for future development of the 3D mosaic.

1) Data quality control

Many users are concerned with details regarding how the data are being quality controlled in the 3D mosaic. There are several QC procedures in the current mosaic. The first one, terrain based GC/Ap removal, uses high-resolution terrain data, in addition to vertical reflectivity continuity and zero velocity check, to identify radar bins that are most likely contaminated by ground clutter. Satellite cloud top temperature data are compared with RUC surface temperature analyses to identify and remove clear air returns and chaff echoes. Simple spatial filters are applied to remove isolated targets and random noise in the reflectivity data. We are continuing to improve the QC scheme by using the Radar Echo Classifier (REC) technique (Kessinger et al. 2003: THE RADAR ECHO CLASSIFIER: A FUZZY LOGIC ALGORITHM FOR THE WSR-88D. 3rd Conference on Artificial Intelligence Applications to the Environmental Science, AMS, 9-13 February 2003, Long Beach, CA). The REC implementation work is scheduled in this year's NAPDT task (04.6.14.5). Other QC technologies including reflectivity climatology and temporal structure based algorithms are under investigation.

2) Gap-filling below the lowest tilt

Large data voids occur in the 3D mosaic grid at lower altitudes especially at far ranges from radar. These voids are a result of NEXRAD scanning strategies and radar beam heights increasing with range due to earth curvature. These data voids pose problems when the data are used in numerical weather prediction models. We have been investigating various options to fill the gaps which include 1) incorporating TDWR data into the Mosaic (NAPDT 2002 4th quarterly report, task 02.6.9), 2) incorporating gap-filling radars such as SMART-R and CASA radars, and 3) extrapolating below the lowest beam using a vertical profile of reflectivity (VPR) approach. These projects, however, are still in research stage and will be carried out through the next a couple of years. The work for incorporating TDWR data in the 3D mosaic is scheduled in this year's NAPDT task 04.6.13.

3) Real-time CONUS domain 3D mosaic: data file size and latency

NSSL is planning to expand the 3D high-resolution mosaic to the CONUS domain with the same spatial and temporal resolution as in the CIWS domain. The national 3D radar mosaic will include ~130 radars from which the NWS will make the base level data available in real-time. Several PDTs including CWPDT, MDEPDT, and Turbulence PDT have shown interest in getting the CONUS 3D mosaic data. Data file size and latency are major concerns when accessing the data in real-time. Estimated size for the CONUS 3D Mosaic grid data is ~0.3GBytes/5min (1km resolution, compressed) in the worst-case scenario (wide spread precipitation everywhere). This is about the same size as the level-II data from all the WSR-88D radars in the network. The latency for mosaicking 10 radars (via the CRAFT) in Oklahoma domain is ~ 1-3min. The latency for the national grid will need to be evaluated when the real-time level-2 data are available from all radars (scheduled for task 04.6.14.2).

04.6.14.2 Enhance the 3D mosaic based on strategies proposed in task 04.6.14.1.

This task starts Jan.1, 2004.

04.6.14.3 Generate and disseminate 3D mosaic gridded data as requested by PDTs.

The activities for this quarter include continued support of real-time CIWS 3D grid data to the CWPDT and the WWRPDT. Real-time products access and related documents were also provided to MCR federal for a cost benefit study (contact: Howard Eichenbaum).

04.6.14.4 Maintenance and regular updates of the real-time 3-D mosaic in the CIWS region.

The activities for this quarter include continued monitoring of the real-time 3-D mosaic for the CIWS domain. Operational system has been updated and network configurations are modified to meet the NOAA security measures.

04.6.14.5 Implement the NCAR REC algorithm in the pre-process for 3D multi-radar mosaic.

The implementation of the radar echo classifier algorithm is undergoing.

04.6.14.6 Test the REC using archived data/cases.

This task starts July 1, 2004.

04.6.14.7-8 4D dynamic grid development.

This task starts Jan. 1, 2004.

b) Planned Efforts

For the next quarter, implementation of the radar echo classifier code in the 3-D mosaic QC process will continue. New development of the 4-D dynamic grid prototype will begin.

c) Problems/Issues

None.

d) Interface with other Organizations

Provided CIWS domain 3D mosaic products information to the MCR federal (Howard Eichenbaum). A survey was sent to all the AWRP PDTs assessing their needs and/or requests for the high-resolution 3D radar mosaic data.

e) Activity Schedule Changes

None.

04.6.15 WARP Activities

The WARP is integral to AT controller displays. Warp is significant in that it shifts the burden of displaying weather radar returns to an instrument specifically designed as a weather radar: the WSR-88D. However, due to the nature of its mission and hardware, the WSR-88D cannot take the same approaches to data quality control as do the long-range L-band radars currently used by ATC. New approaches to data quality control need to be developed so the users have confidence in the weather data products displayed to them.

a) Current Efforts

A median filter is used by the AP mitigation technique in ORPG composite reflectivity products to expand on the identification of AP using single gate analysis. It is considered likely that other gates are AP if enough of the neighbors in the filter window are also AP. Currently, the median filter calculates a new averaged reflectivity value at a gate regardless of whether the data point is determined to be precipitation or AP. Thus, the filter acts to smooth out reflectivity returns in areas of precipitation producing a reduction in reflectivity intensities. This result has produced noticeable differences in the reflectivity intensities of products with (ORPG product 36) and without (ORPG product 96) AP mitigation.

A solution to this problem is realized by calculating a new averaged reflectivity value only if the median filter determines a data point to be AP. Hence, reflectivity values within precipitation regions are not adjusted by the filter. This modification has been applied to all data cases examined in Smalley and Bennett (2001). Smalley and Bennett originally investigated the AP mitigation technique and adjusted an adaptable parameter set so that the median filter could produce optimal results in a variety of AP cases.

By modifying reflectivity values only in non-precipitation regions of the reflectivity field, AP is still properly removed while reflectivity intensities associated with precipitation are not reduced. An archive of the AP and convective cases using the current version of ORPG product 96 and the modified version of product 96 is being kept at http://www.cimms.ou.edu/~porter/warp.

The ORPG Fortran code has been modified to institute the changes within the median filter. Only 3 lines of new code are needed while commenting out one previously existing line of code. Thus, the modification is extremely simple and actually reduces the amount of CPU time needed to produce ORPG product 96 by bypassing a portion of the median filter code when precipitation returns are being examined.

Because the current version of the median filter smooths reflectivity data, results of the modification are particularly dramatic for convective cases that contain relatively small maximum reflectivity cores on the order of 10 to 20 km

with sharp reflectivity gradients. Two of the archived examples are provided below.

Figs. 3-5 show ORPG product 36 (Fig. 3), ORPG product 96 (Fig. 4), and the

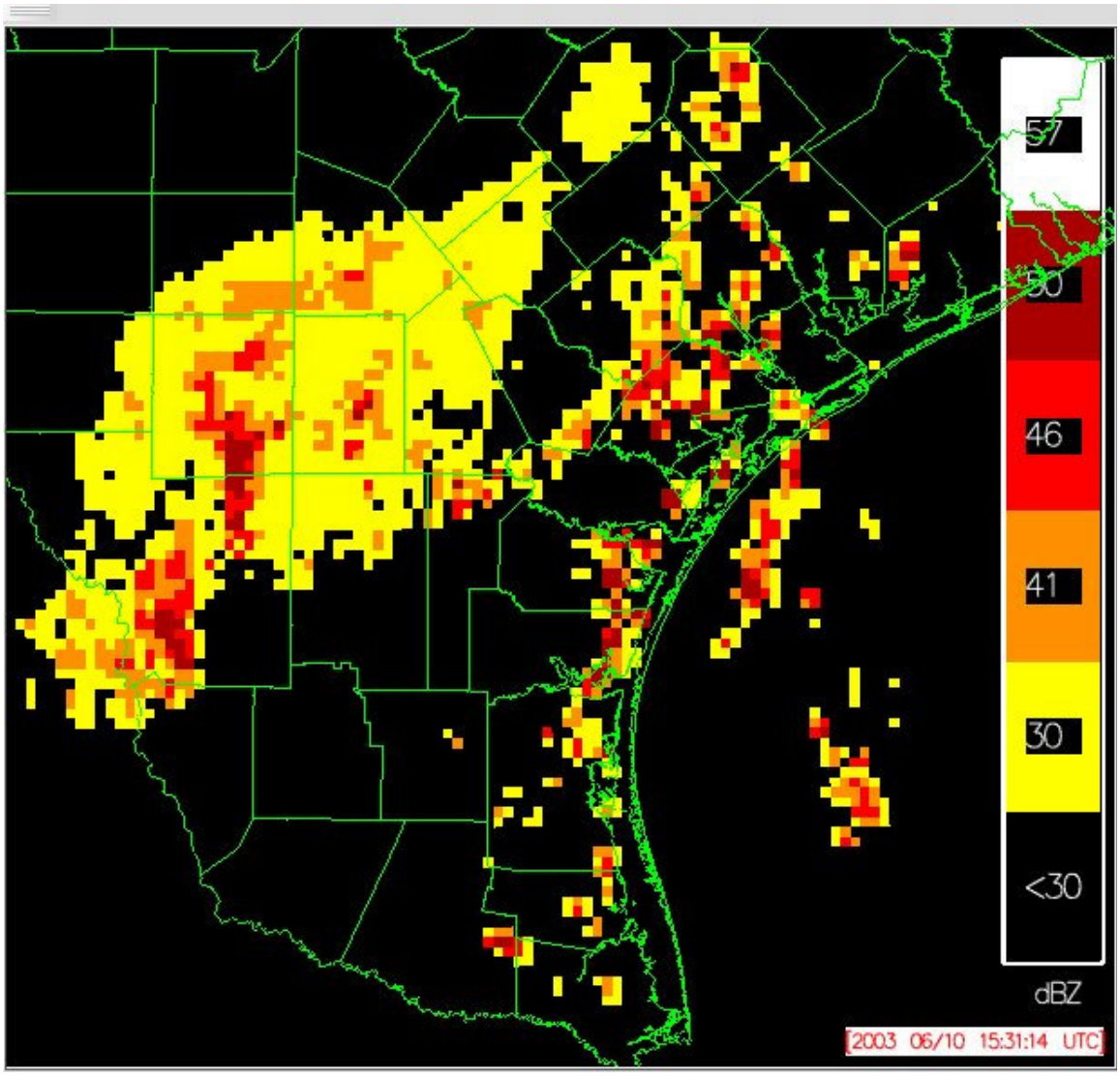

Figure 3. ORPG Composite Reflectivity Product 36 output for the Corpus Christi, TX (KCRP) WSR-88D radar at 1531 UTC, June 10, 2003.

modified version of product 96 (Fig. 5) for a convective case at Corpus Christi, TX (KCRP) on June 10, 2003 at 1531 UTC. There is very little AP in this case. However, the smoothing effect of the median filter is obviously seen in the convective cells along the Texas coastline (Figure 1b) with many reflectivity values reduced by 10 to 20 dB. When the median filter is only applied in non-precipitation areas, the original reflectivity values within the storm cells are retained (Figure 1c).

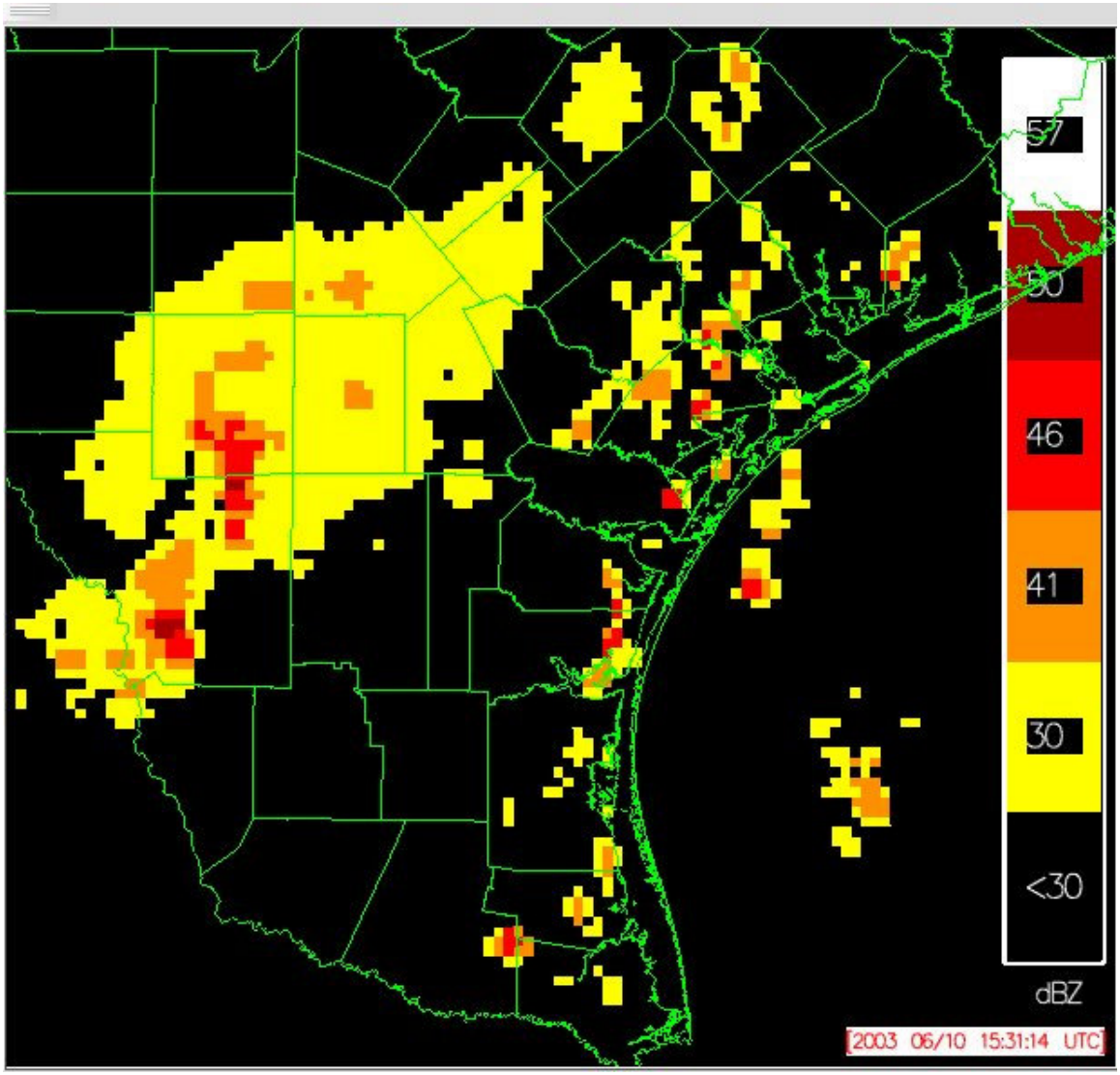

Figure 4. Same as Fig. 3 except for the ORPG AP-edited Composite Reflectivity Product 96.

Figs. 6-8 shows the same ORPG products as in Figs. 3-5, but for an AP case surrounding the Ft. Worth (KFWS) WSR-88D on October 1, 1997 at 1543 UTC. Several convective cells are contained within widespread AP across north Texas (Fig. 6). Both ORPG product 96 (Fig. 7) and the modified version of product 96 (Fig. 8) remove much of the AP. However, the modified product retains the original reflectivity values within the convective cells that are reduced by 10 to 20 dBZ within the current product 96.

Five more cases in addition to these two are archived at the website given above. Although maybe not as dramatic as the examples given here, the other cases also show that AP is still effectively removed using the modified version of ORPG product 96 while retaining the original, and sometimes critical, reflectivity information within convective cells.

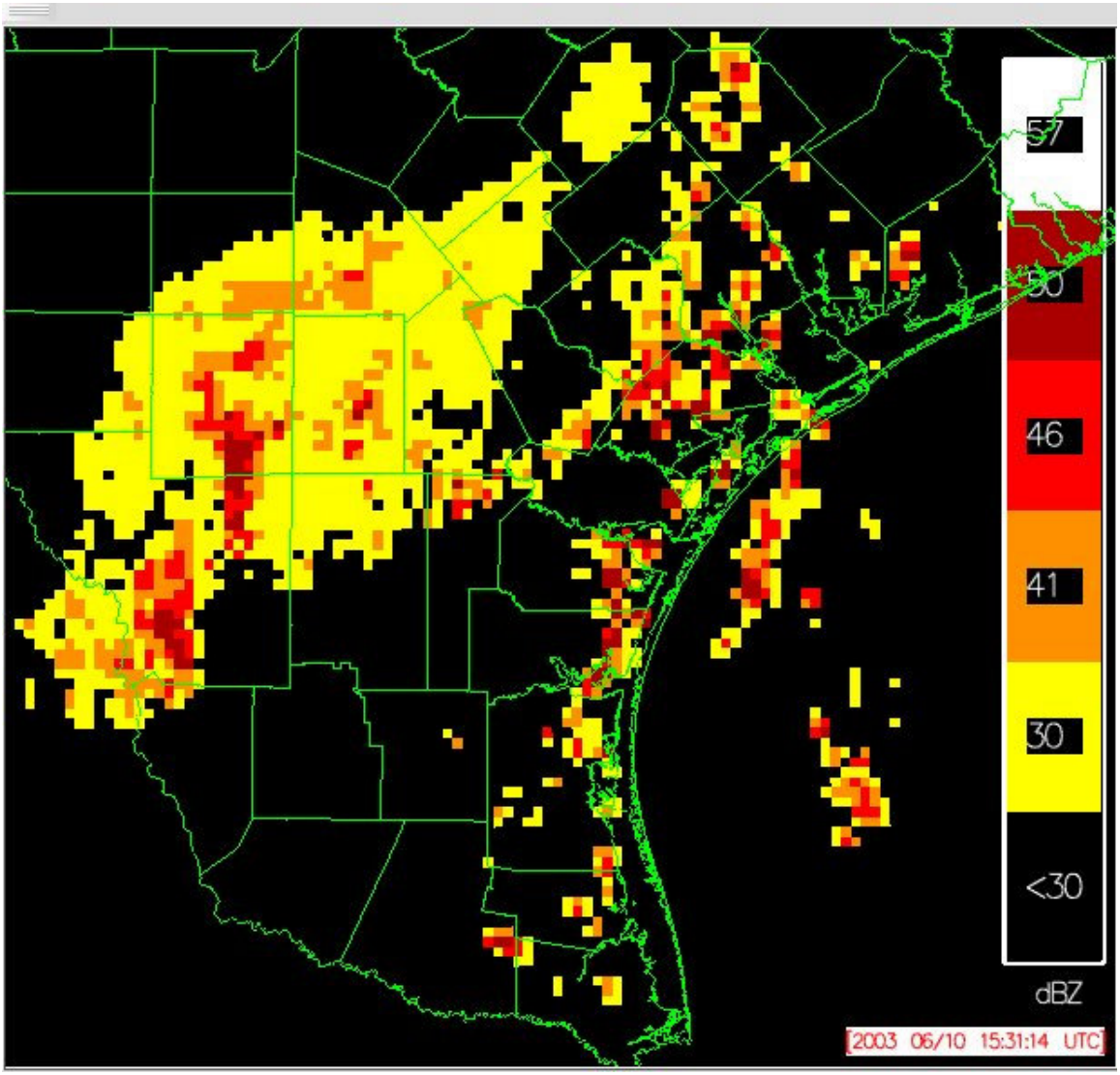

Figure 5. Same as Fig. 4 except that the median filter is only used when analyzing AP data points.

b) Planned Efforts

Continue investigation of data quality issues as pertains to WARP applications.

c) Problems/Issues

None.

d) Interface with other Organizations

None.

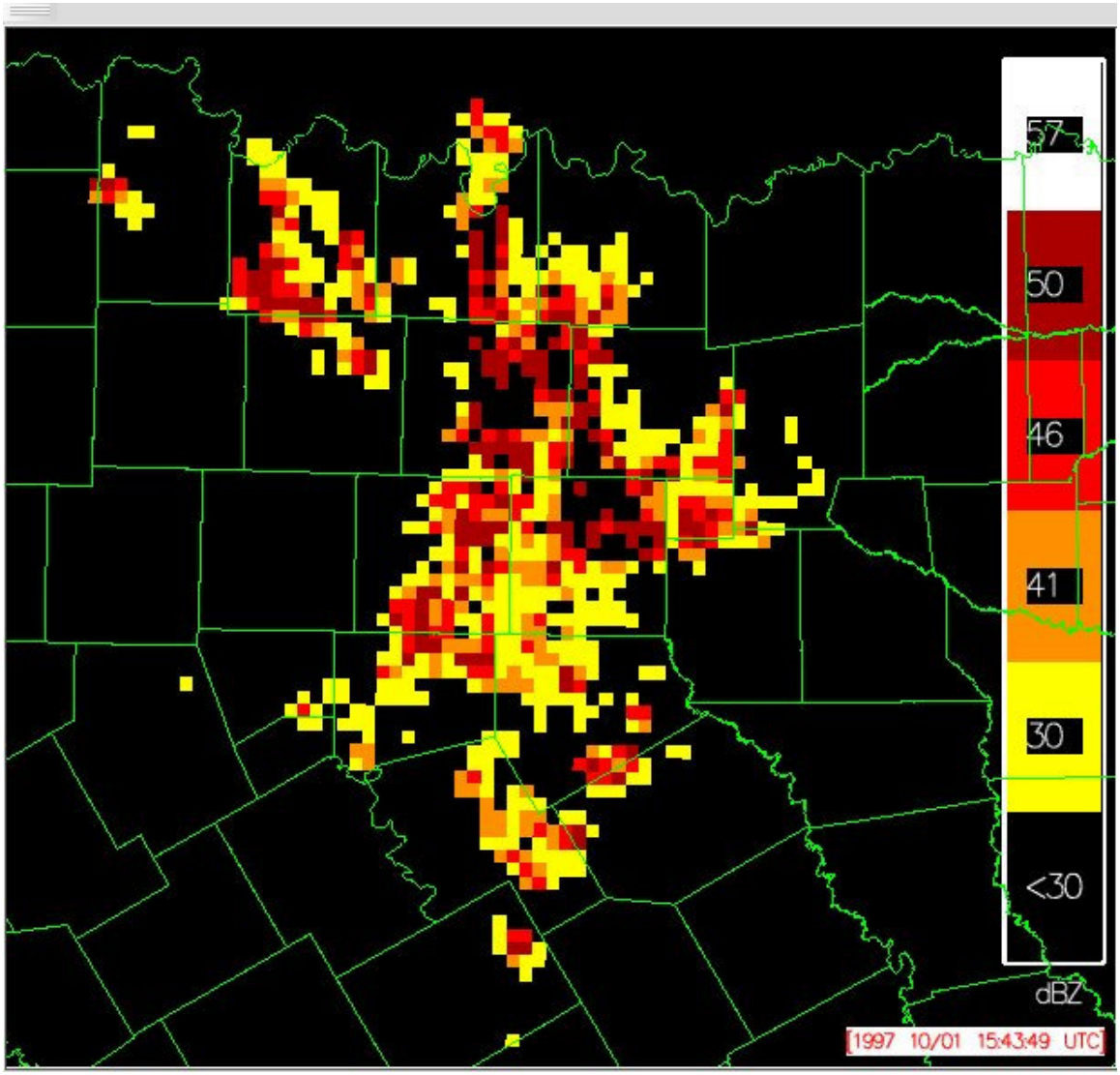

Figure 6. ORPG Composite Reflectivity Product 36 output for the Forth Worth, TX (KFWS) WSR-88D radar at 1543 UTC, October 1, 1997.

e) Activity Schedule Changes

None.

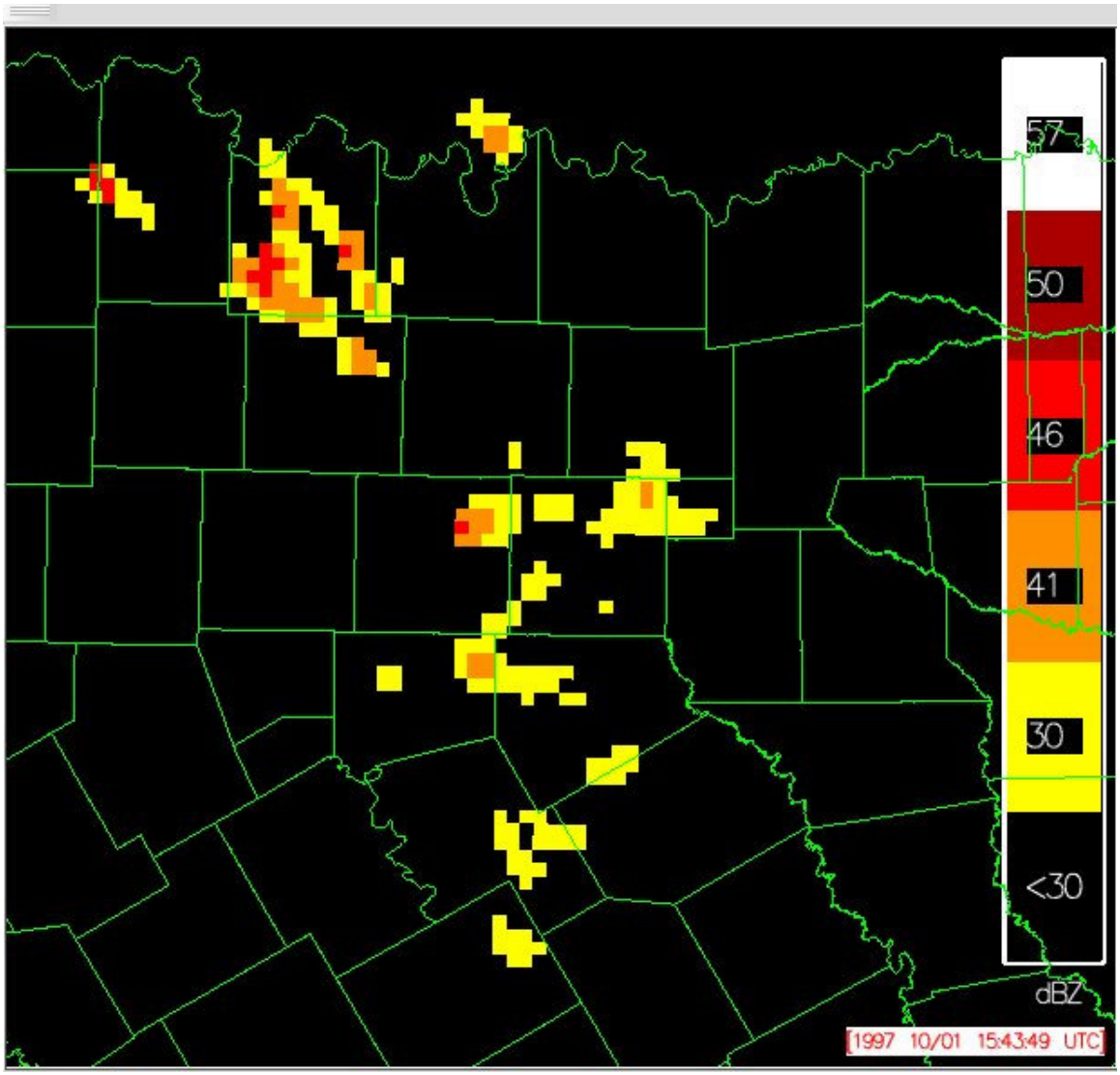

Figure 7. Same as Fig. 6 except for the ORPG AP-edited Composite Reflectivity Product 96.

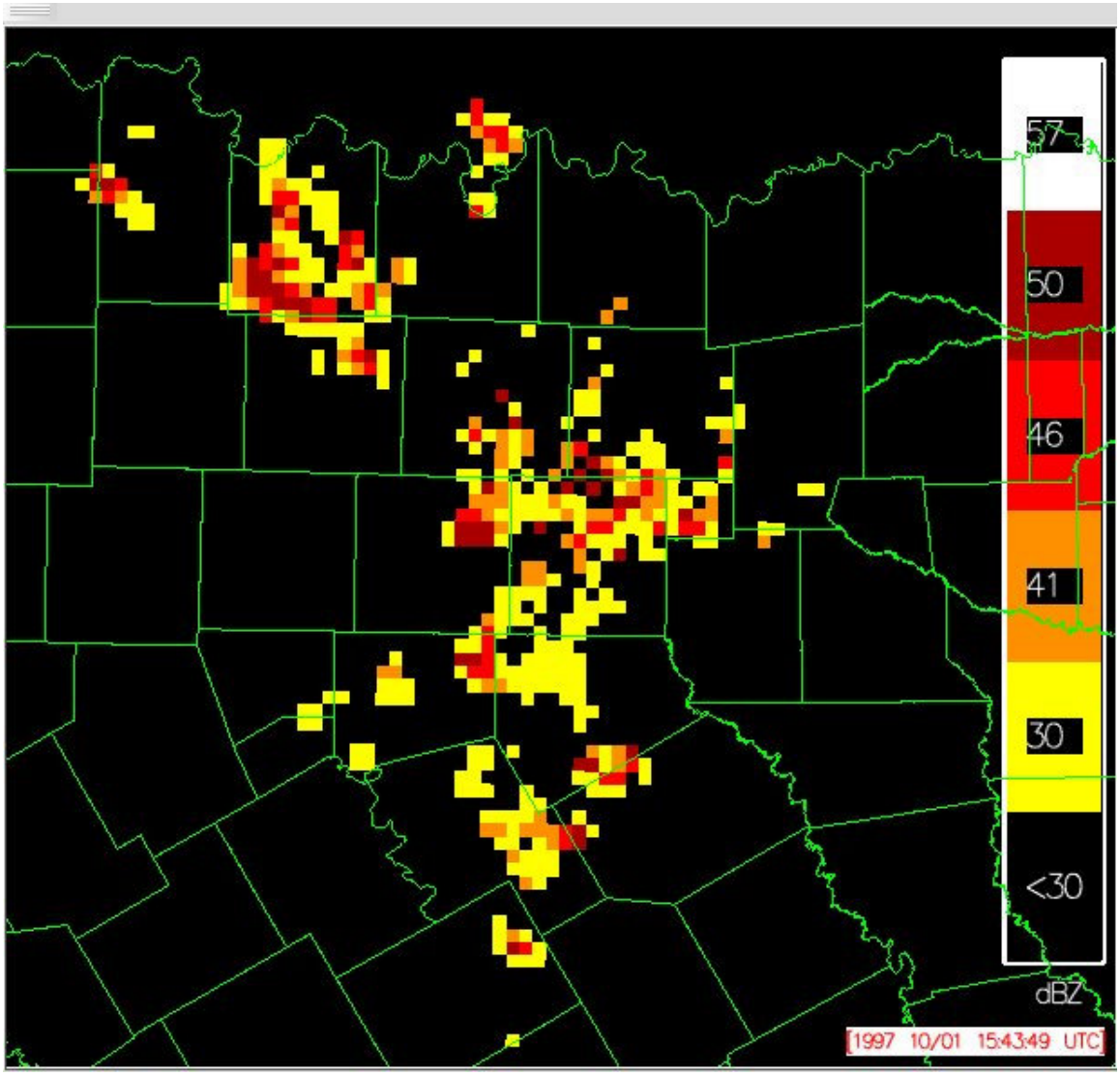

Figure 8. Same as Fig. 7 except that the median filter is only used when analyzing AP data points.

Appendix 1

Radar data quality improvement: Calibration issues of dual-polarization measurements.

1. Introduction

Radar calibration is essential to producing high quality weather radar data, particularly for rainfall measurements. Most recent reviews of different techniques for calibration of radar reflectivity factor Z can be found in Joe and Smith (2001) and Atlas (2002). The reviews concluded that after several decades of research in radar meteorology, we still have serious problems with Z calibration on operational radars. Bolen and Chandrasekar (2000) found variability in the calibrations of the NEXRAD WSR-88D radars with respect to the NASA TRMM satellite radar that can be used as a traveling standard against which ground-based weather radars can be calibrated. Recent findings of Gourley et al. (2003) also indicate that the 2 – 3 dB discrepancy between reflectivities measured by adjacent WSR-88D radars is quite common.

In coming years, many operational weather radars in the US and other countries will be upgraded by adding polarimetric capability. Polarization diversity might help to improve the quality of radar reflectivity calibration. Goddard et al. (1994) and Gorgucci et al. (1999) expressed the idea that two polarimetric variables, differential reflectivity Z_{DR} and specific differential phase K_{DP}, and radar reflectivity Z are not independent in rain medium, therefore, Z can be roughly estimated from Z_{DR} and K_{DP}. The difference between computed and measured values of Z is considered a Z bias. Recent studies of Illingworth and Blackman (2002) and Vivekanandan et al. (2003) claim that the accuracy of Z calibration based on the consistency among the three radar variables can be as good as 0.5 to 1 dB.

Although these findings are encouraging, there are several issues that have to be clarified and resolved prior to practical utilization of the suggested technique. One of them is sensitivity of a "self-consistency" relation to the drop size distribution (DSD) variations and uncertainty in raindrop shape and canting. Also, it is not clear how to use this methodology for relatively light precipitation where K_{DP} estimates are very noisy.

2. Calibration of Z based on polarimetric self-consistency.

a. Consistency principle

According to the consistency principle, radar reflectivity factor in rain can be roughly estimated from Z_{DR} and K_{DP} using the following relation

$$Z = a + b \log(K_{DP}) + c\, Z_{DR} \quad , \qquad (1)$$

where Z is expressed in dBZ, Z_{DR} – in dB, and K_{DP} – in deg/km. The coefficients a, b, and c in (1) depend on a radar wavelength, prevalent raindrop shape, and are supposed to be relatively insensitive to the DSD variations. The consistency principle is formulated in a slightly different way by Goddard et al. (1994) and Illingworth and Blackman (2002).

They claim that the ratio of K_{DP} and Z (expressed in mm^6m^{-3}) is a well-defined function of Z_{DR} and is virtually independent of DSD variations.

Since K_{DP} can be quite noisy, especially in light rain, Goddard et al. (1994) recommended to express K_{DP} as a function of Z and Z_{DR} and examine its integral, the total differential phase

$$\Phi_{DP}^{est}(R) = 2\int_0^R K_{DP}(Z, Z_{DR})\,dr \qquad . \qquad (2)$$

Radial profile of the measured differential phase Φ_{DP} is then compared to the radial profile of estimated differential phase Φ_{DP}^{est}. If the radar is perfectly calibrated then the two radial profiles should be very close to each other in rain medium. The mismatch between these two profiles indicates possible calibration error of Z. This error can be determined as an adjustment to Z that is required to match the two profiles of differential phase. This method works only if differential phase is sufficiently large.

Working with the JPOLE polarimetric data we found out, that although the idea of the Z calibration based on self-consistency is quite viable, there are serious methodological problems with practical implementation of this idea in operational environment. First of all, there are several consistency relations available in literature. They were obtained with different assumptions about DSDs and raindrop shapes, and produce noticeably different results in estimation of the Z bias. The discrepancy might point to the fact that the consistency technique is much more affected by uncertainty in DSDs and raindrop shapes than was previously thought.

Another stumbling block is a procedure for "matching" the measured and estimated radial profiles of Φ_{DP} which was not implicitly described in any of the referred literature sources. It is clear that differential phase should be sufficiently large to make such "matching" possible. This automatically excludes many rain events with relatively low maximal values of Φ_{DP} (e.g., stratiform or isolated convective precipitation) from the list of suitable targets for such calibration. In the presence of hail, the consistency relations become invalid and this factor diminishes even more the number of radials appropriate for calibration.

b. Modified consistency technique for calibration of Z

During JPOLE experiment, we applied different consistency relations from the literature to calibrate radar reflectivity factor measured by the KOUN WSR-88D radar. The results of the Z calibration have been validated by comparisons with Z measurements from the operational KTLX WSR-88D radar, which is supposed to be well calibrated. Unfortunately, different consistency relations yield quite different results for the Z bias estimate that can differ by few dB. Neither one provides an agreement within 1 dB with the results of direct comparisons of reflectivities obtained from the KTLX and KOUN radars.

These discrepancies can be partially explained by the fact that the consistency technique is likely more prone to the DSD diversity that was originally thought. Different authors derived the consistency relations based on different assumptions about DSD variations and raindrop shape. Oklahoma (and Great Plains in general) is notorious for extreme variability of rain types and associated DSDs. Therefore, it is not surprising that the set of model DSD does not always match well the actual DSD in precipitation.

Analysis of 24 rain events (50 hours of observations) observed during several months of JPOLE reveals at least two different dominant rain regimes in Oklahoma. The $Z - Z_{DR}$ scatterplots or dependencies displayed for particular hour of observations in the watershed – sized area serve as very good indications of the rain type and corresponding DSD. Fig. 1 illustrates such mean $Z - Z_{DR}$ dependencies for each of 50 hours of radar observations in the 50 x 40 km area containing 42 Agricultural Research Service Micronet rain gages. Two major clusters of curves (red and green) represent two prevalent rain regimes. One of them (red curves) is characterized by larger drop sizes and is associated primarily with warm-season convection, whereas the other one (green curves) is typical for cold-season stratiform rain with abundance of smaller drops. Very often these two rain types coexist in one precipitation event or they can gradually evolve into each other during lifetime of a particular storm. Few outliers are evident among the $Z - Z_{DR}$ dependencies (blue curves). Some of them are attributed to the storms that produce big hail and very large raindrops originated from melting hail. These situations are characterized by extremely large Z_{DR}s that might be combined with modest values of Z. Another extremity is represented by a couple of tropical rain events with very high concentrations of small drops. In tropical rain, Z_{DR} is usually anomalously low even for high reflectivities.

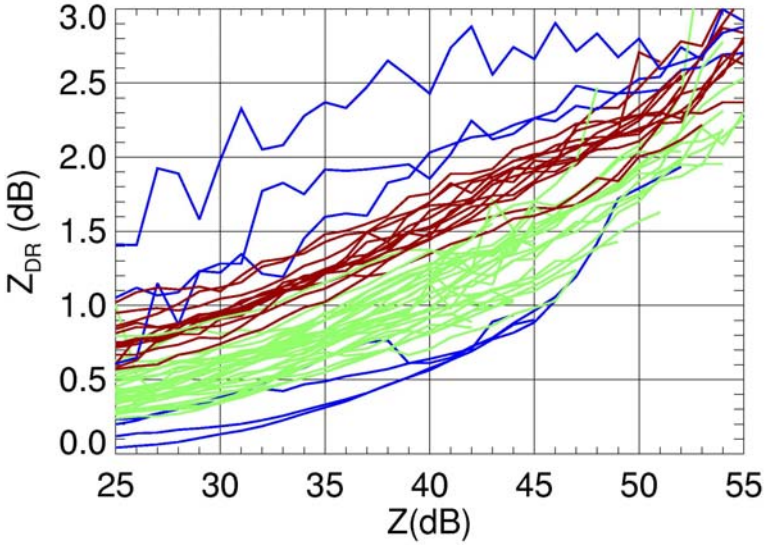

Fig. 1 The $Z - Z_{DR}$ dependencies for each of the 50 hours of rain observations during JPOLE. Different colors denote different rain regimes.

Given the problems encountered and the complexity of real-life situation we significantly modified the polarimetric consistency technique for calibration of Z. Three principle changes have been made.

(1) We used two consistency relations obtained from the data rather than the one retrieved from the model simulations. They are

$$Z = 46.1 + 14.4 \log(K_{DP}) + 1.23\, Z_{DR} \qquad (3)$$

for "convective" type of rain and

$$Z = 49.8 + 11.3 \log(K_{DP}) - 0.78\, Z_{DR} \qquad (4)$$

for "stratiform" type of rain. Thus, two Z bias estimates are computed concurrently. The choice of a right one is made from the comparisons of the $Z - Z_{DR}$ and $K_{DP}/Z - Z_{DR}$ dependencies obtained from the data with the model dependencies for the "convective" and "stratiform" types of rain. If the measured Z (after correction) , Z_{DR}, and K_{DP} match well the "convective" curves, then the estimate (3) is selected. The estimate (4) is chosen if there is a good match with the "stratiform" curves. Both estimates are considered unreliable if there is no good match with both models. In operational practice the radar constant may change abruptly but usually remain stable for long periods of time. Therefore, we can always wait long enough before the appropriate rain type with DSD close to either "convective" or "stratiform" model is observed in a sufficiently large spatial / temporal domain.

(2) The consistency relations are valid only in rain, therefore regions of hail and non-meteorological echoes should be identified and excluded from consideration. We are doing such assessment on the radial-by-radial basis using the polarimetric classification routine described in the October 2003 FAA report and in Schuur et al. (2003).

(3) Instead of examining individual radial profiles of differential phase, we calculate areal-time integrals of the measured K_{DP} and computed $K_{DP}(Z,Z_{DR})$ and match them by adjusting Z. Only pixels (or gates) containing rain are counted in such integration. There is plenty of flexibility in selecting particular area and time intervals for integration. In our analysis we normally use the test area 50 x 40 km encompassing the ARS Micronet gages and standard one-hour time interval. The advantage of this approach is that by integration of specific differential phase over large space-time domain we substantially reduce the inherent noisiness in the K_{DP} estimates.

c. Results of polarimetric calibration of Z during JPOLE.

For each of 50 hours of radar observations when noticeable rain accumulations were recorded by gages in the ARS area, we performed calibration of the KOUN radar using two methods. One of them implies direct comparisons of the reflectivities measured by the KOUN and KTLX radars. In fact, we estimated hourly areal rain totals from the KOUN and KTLX reflectivity data and calculated the needed adjustment to the Z measurements from the polarimetric radar to match these two estimates. Independent estimate of the Z bias for the KOUN radar was obtained from the KOUN polarimetric data using the modified self-consistency technique described in the previous section.

Out of 24 days of observations, we selected 13 days for which we have very strong confidence in the results of the self-consistency calibration and direct comparisons of reflectivities from the two radars. The results are summarized in Table 1 and Fig. 2. Both estimates of the Z bias for the KOUN radar agree quite well except for the case on 06/12/03 for which we are not very confident in the $Z_{KOUN} - Z_{KTLX}$ value (5.4 dB). The RMS difference between the two estimates is 1.1 dB for 13 days and 0.8 dB if the outlier case is excluded. Very good agreement is achieved for light stratiform rain (cases 5, 6, and 7) despite high noisiness of the K_{DP} data. As Fig. 2 shows, both methods indicate very similar temporal trends in the sign and degree of the Z mis-calibration on the KOUN radar. It is not possible to say which technique is more accurate in terms of absolute

calibration (because the KTLX radar might be mis-calibrated itself) but the fact that they produce consistent results proves efficiency of the self-consistency polarimetric approach that does not require a reference radar.

Table 1. Results of the self-consistency polarimetric calibration (ΔZ_{KOUN}) and their validation from direct comparison of reflectivities from the KOUN and KTLX WSR-88D radars ($Z_{KOUN} - Z_{KTLX}$) for different days of observations during JPOLE.

Case number	Date	$Z_{KOUN} - Z_{KTLX}$ (dB)	ΔZ_{KOUN} (dB)
1	06/13/02	-4.1	-2.6
2	06/16/02	-2.0	-2.9
3	08/14/02	-1.2	-0.8
4	09/14/02	-2.2	-1.9
5	10/08/02	2.8	3.7
6	10/09/02	3.1	3.7
7	10/24/02	3.5	3.6
8	10/28/02	3.2	3.5
9	04/19/03	-1.6	0.1
10	05/20/03	-0.3	-0.6
11	06/06/03	2.2	2.6
12	06/12/03	5.4	2.9
13	06/13/03	4.4	4.4

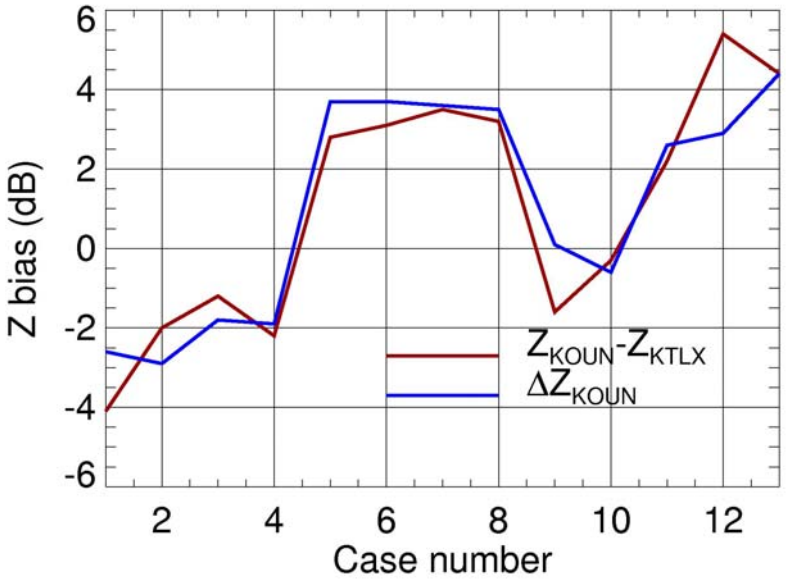

Fig. 2. The bias of reflectivity measurements by the KOUN WSR-88D radar as a function of the day of observations ranked in chronological order. ΔZ_{KOUN} is the estimate from the polarimetric self-consistency method and $Z_{KOUN} - Z_{KTLX}$ is the difference between reflectivities measured by the KOUN and KTLX WSR-88D radars.

3. References

Atlas, D., 2002: Radar calibration: some simple approaches. *Bull. Amer. Meteor. Soc.,* **83**, 1313 – 1316

Bolen, S.M, and V. Chandrasekar, 2000: Quantitative cross validation of space-based and ground-based radar observations. *J. Appl. Meteor*., **39**, 2071 – 2079.

Goddard, J., J. Tan, and M. Thurai, 1994: Technique for calibration of meteorological radars using differential phase. *Electronic Letters*, **30**, 166 – 167.

Gorgucci, E., G. Scarchilli, and V. Chandrasekar, 1999: A procedure to calibrate multiparameter weather radar using properties of the rain medium, *IEEE Trans. Geosci. Remote Sensing*, **37**, 269 – 276.

Gourley, J., B. Kaney, and R. Maddox, 2003: Evaluating the calibrations of radars: a software approach. Preprints*, 31st International Conference on Radar Meteorology,* Seattle, 459 – 462.

Illingworth, A., and T. Blackman, 2002: The need to represent raindrop size spectra as normalized Gamma distributions for the interpretation of polarization radar observations. *J. Appl. Meteorol.*, **41**, 286 – 297

Joe, P., and P.L. Smith, 2001: Summary of the Radar Calibration Workshop. Preprints*, 30tht International Conference on Radar Meteorology,* Munich, Germany, 174 – 176.

Schuur, T., A. Ryzhkov, P. Heinselman, D. Zrnic, D. Burgess, and K. Scharfenberg, 2003: Observations and classification of echoes with the polarimetric WSR-88D radar. NSSL report, 46 p.

Vivekanandan, J., G. Zhang, S. Ellis, D. Rajopadhyaya, and S. Avery, 2003: Radar reflectivity calibration using differential propagation phase measurement. *Radio Science*, **38**, No 3, MAR 14-1-14.

Appendix 2:

Infrastructure support tasks accomplished in the 1st Quarter 2004

1. Ingest of Phased Array Radar Data

We can now ingest radar data in Universal Format for displays and algorithms. This is particularly helpful because at least initially, all the data from the phased array radar is being distributed in Universal Format. Shown are some of the first images from the phased array radar after it was handed off to NSSL from Lockheed Martin.

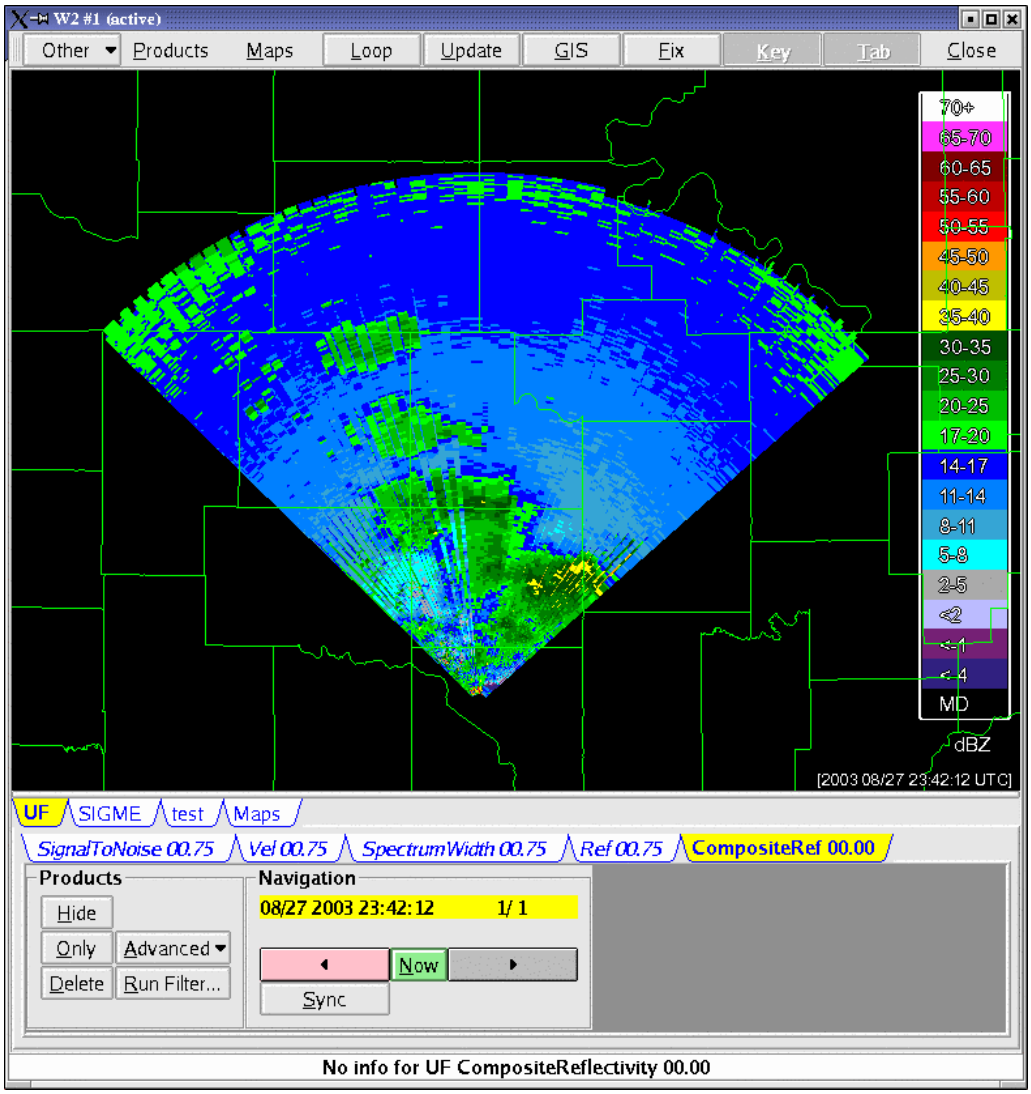

Figure 1: Composite Reflectivity product from the phased array radar

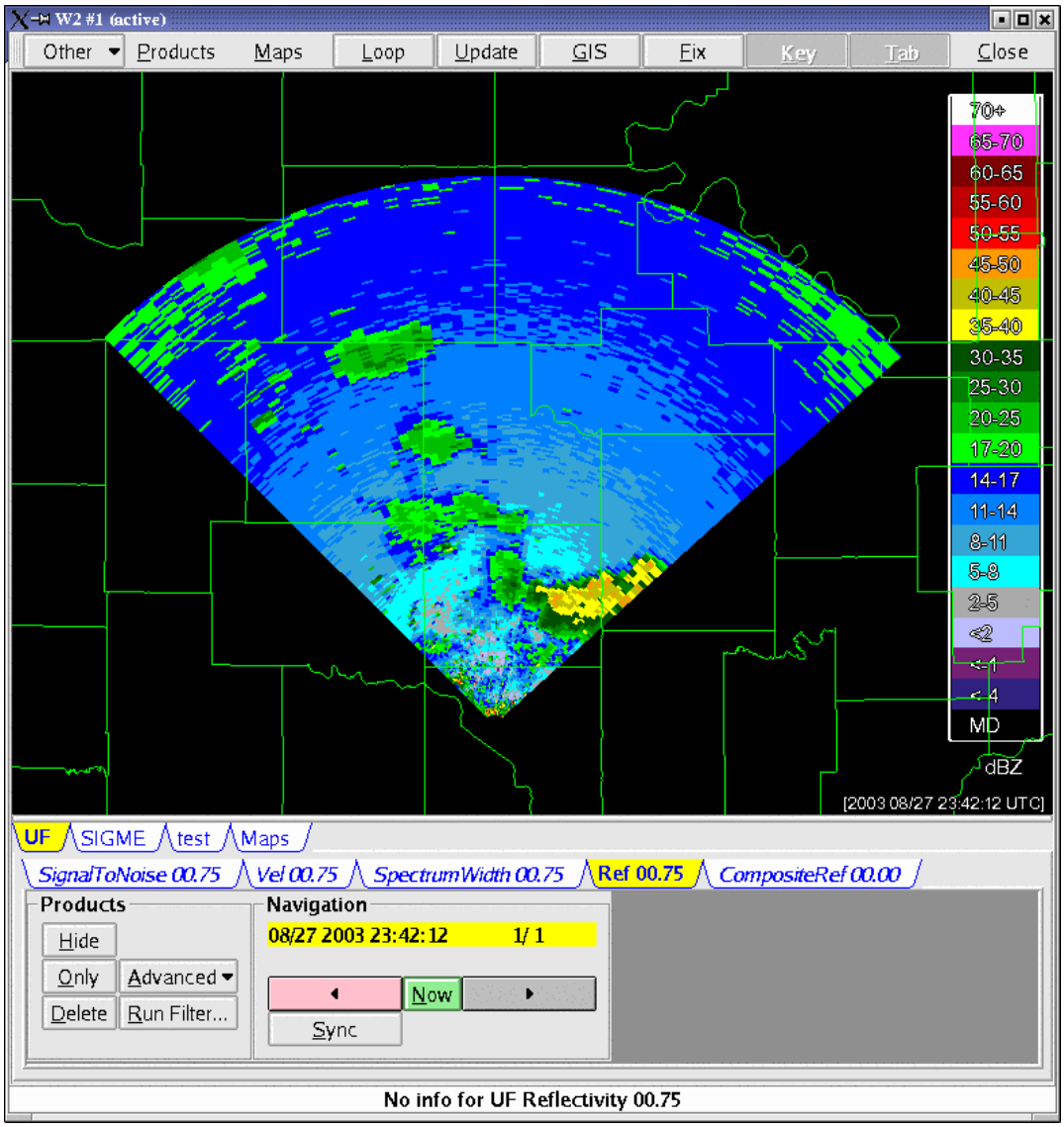

Figure 2: Reflectivity sweep at 0.75 degrees. Because the beams are electronically steered, some of the beams (those pre-programmed as hitting water towers, etc.) are nearly vertical, and have to be removed before display.

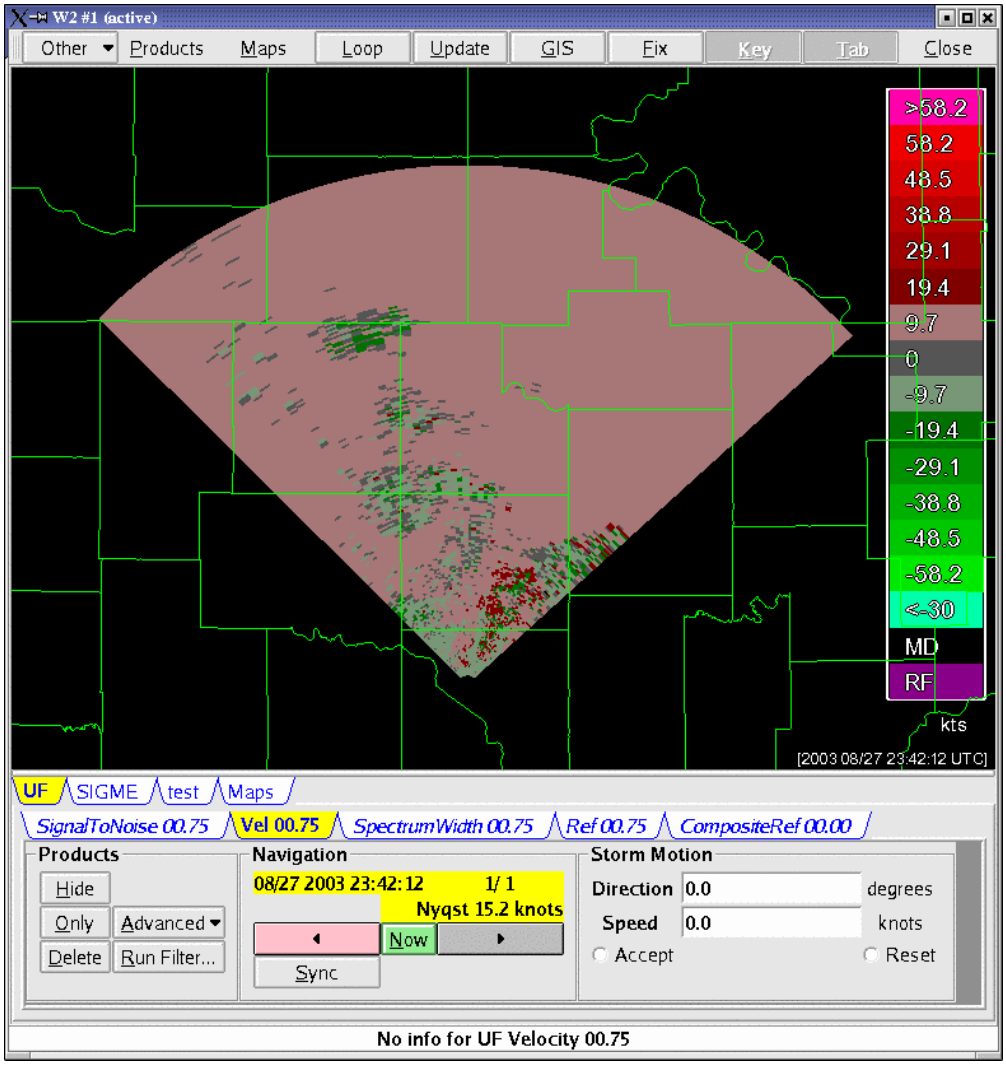

Figure 3: Doppler velocity from the phased array radar.

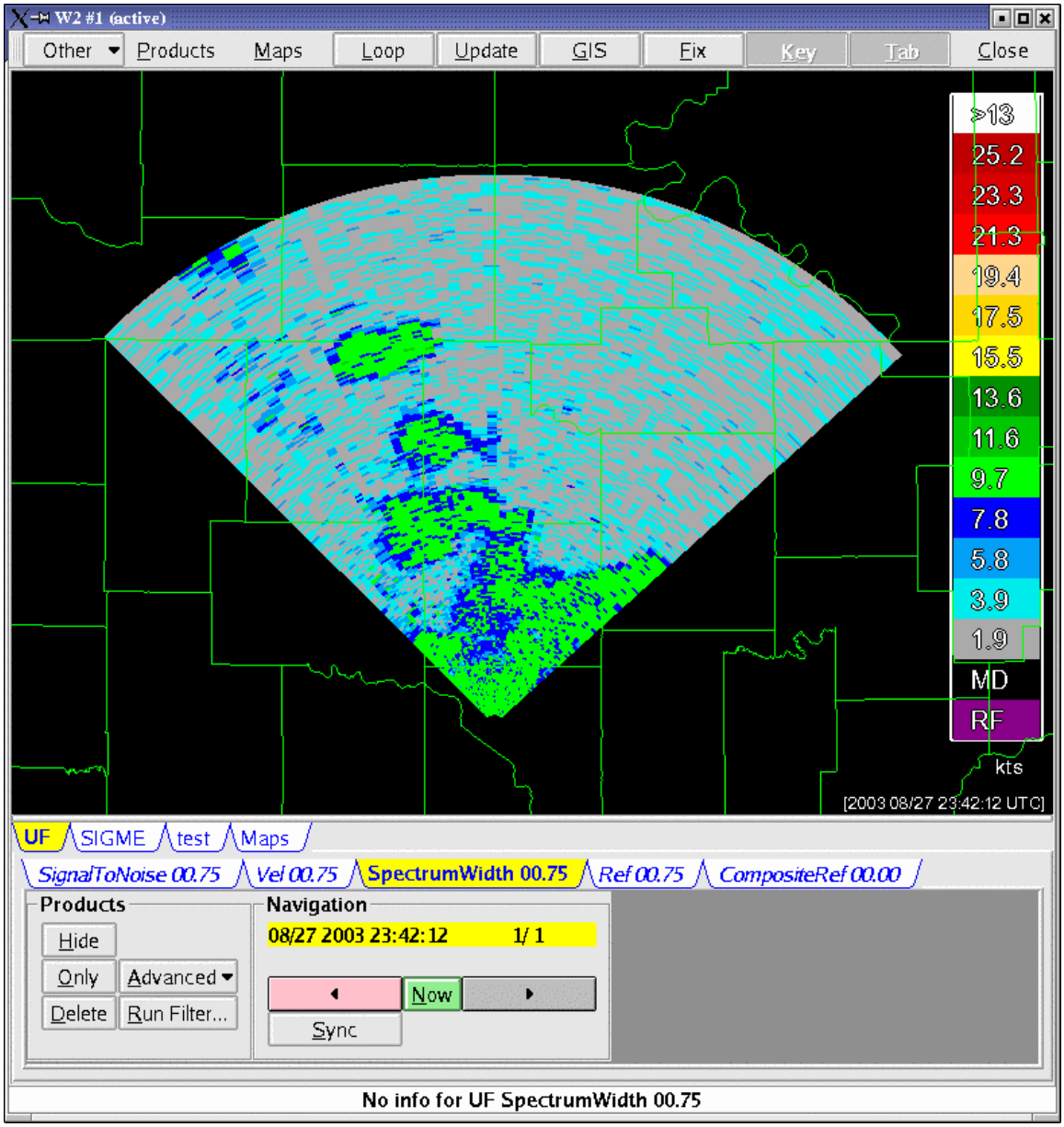

Figure 4: Spectrum width product from the phased array radar.

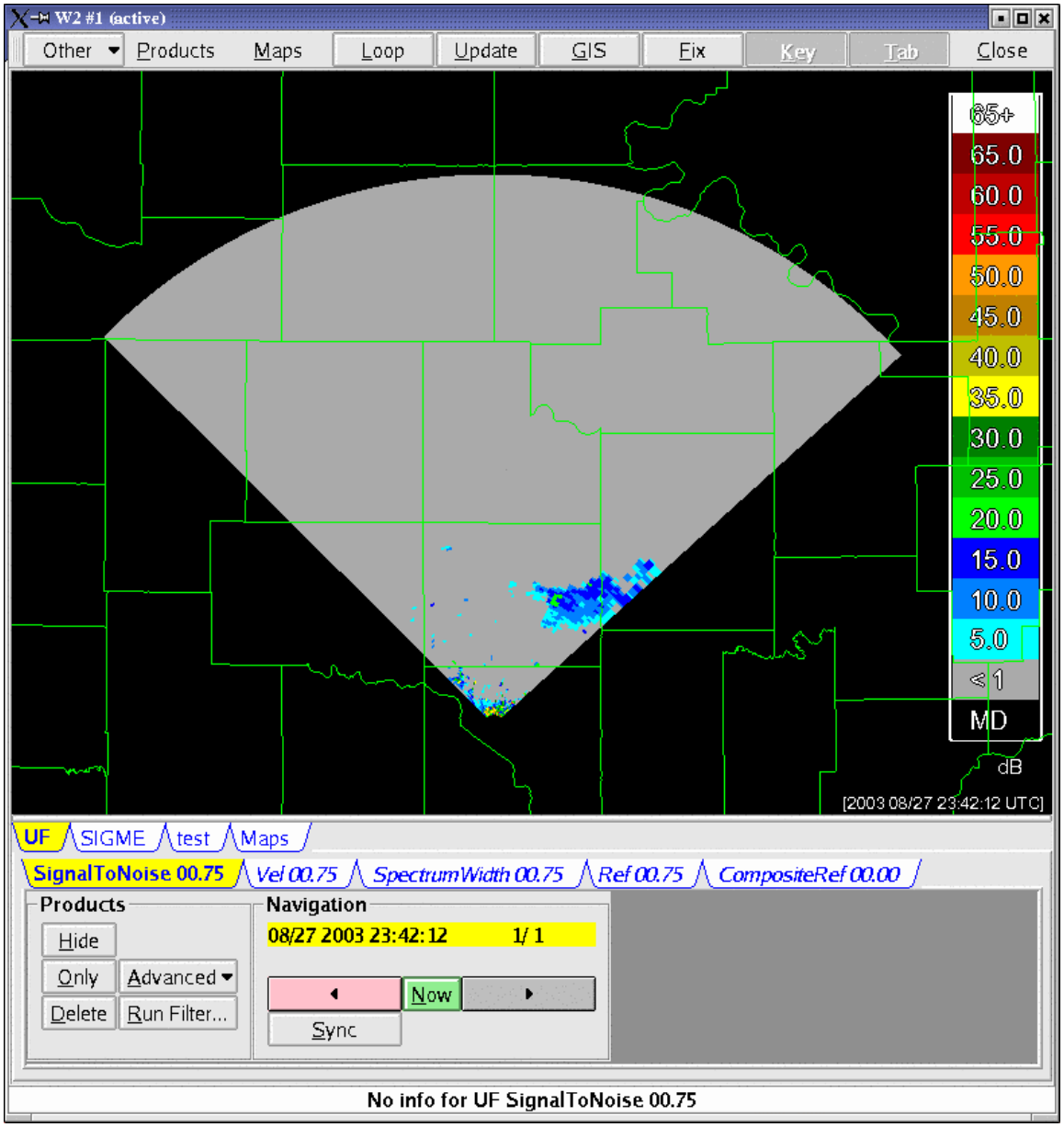

Figure 5: Signal-to-noise ratio from the phased array radar

It is clear that at least for the present, the phased array radar is being run in conventional radar scanning patterns. We will continue to support the ingest and display of phased array radar data as it gets more creative.

2. Next generation of Display program

With the testing of our display software last spring, we received many suggestions on how to make the software more intuitive, and ideas for more features. We are incorporating many of these ideas into a complete redesign of the display interface.

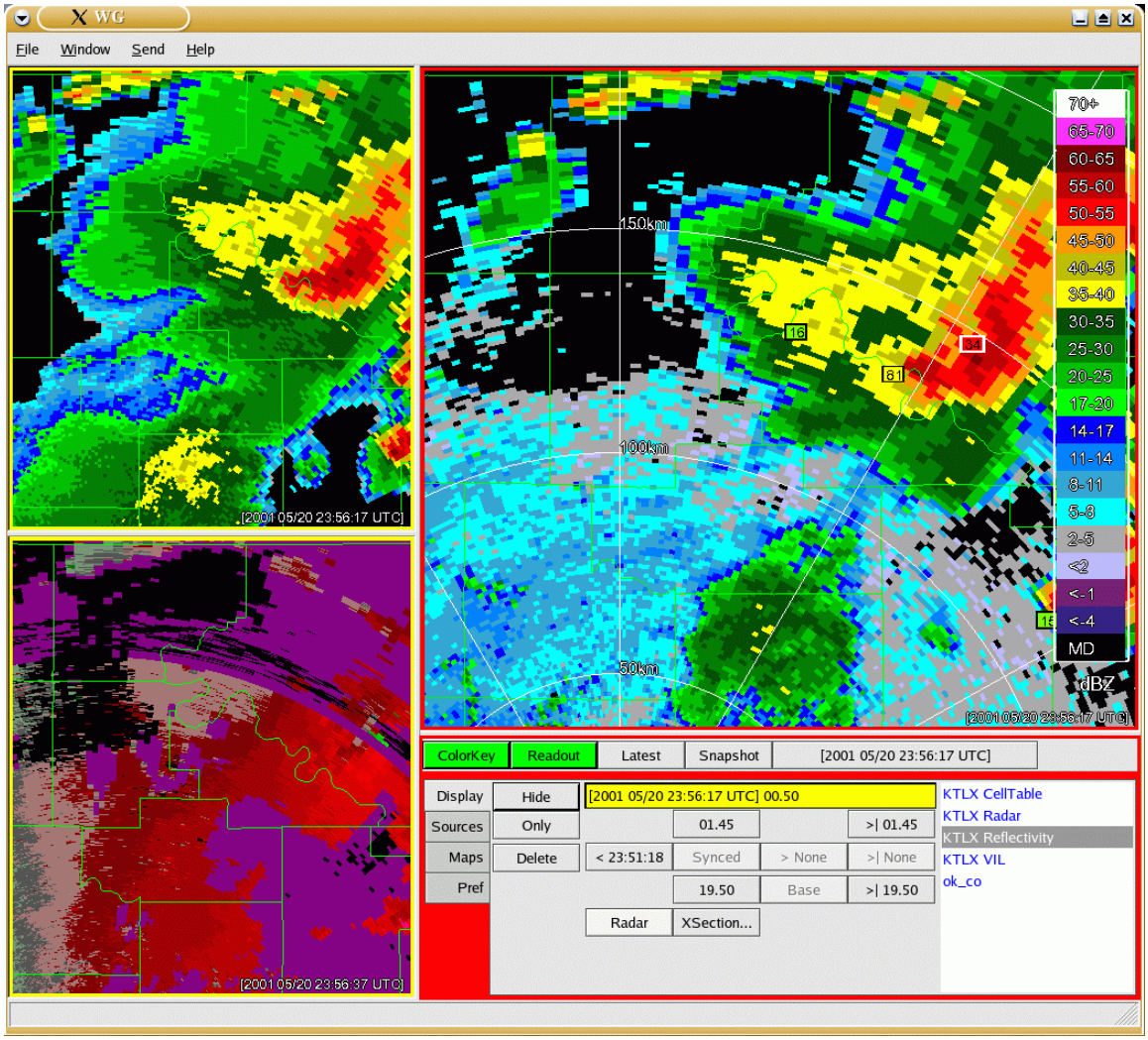

Figure 6: Redesigned interface to display program

The redesigned display already supports these features:

- Display of gridded (polar, Cartesian, lat-lon) data from radar, satellite, and merged radars.
- Display of icon-type products including mesonet and lightning.
- Linked cursors
- Maps and overlay editing
- Improved time and elevation navigation.
- Virtual volume navigation capability.
- Data readout in the user's choice of units (metric/English)

3. Ingest and display of SMART-R data

We can now ingest data in the SIGMET processor format used by SMART-R radars. Any data that can be visualized within WDSS-II can be used as inputs to the algorithms as well.

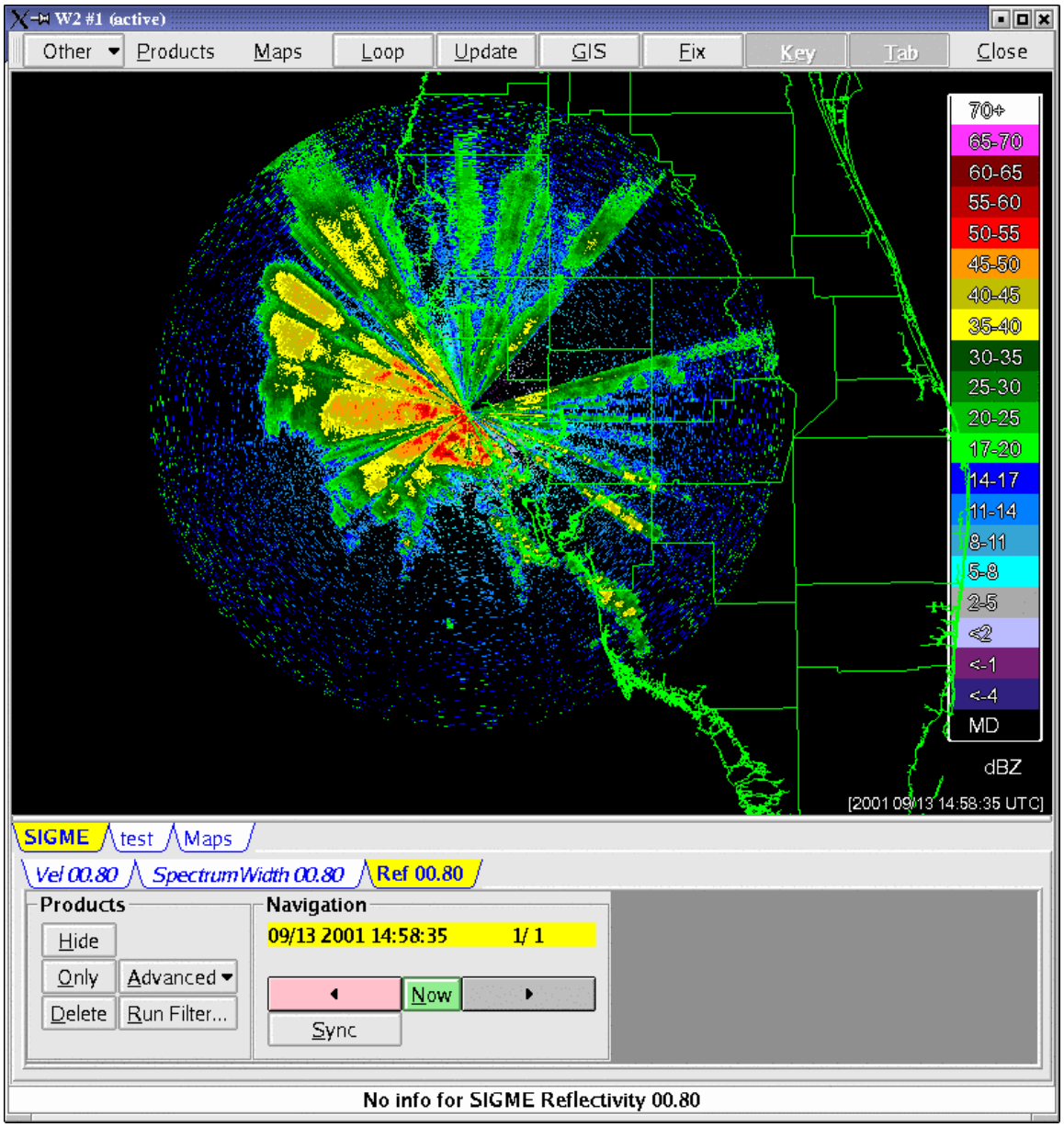

Figure 7: SMART-R reflectivity sweep

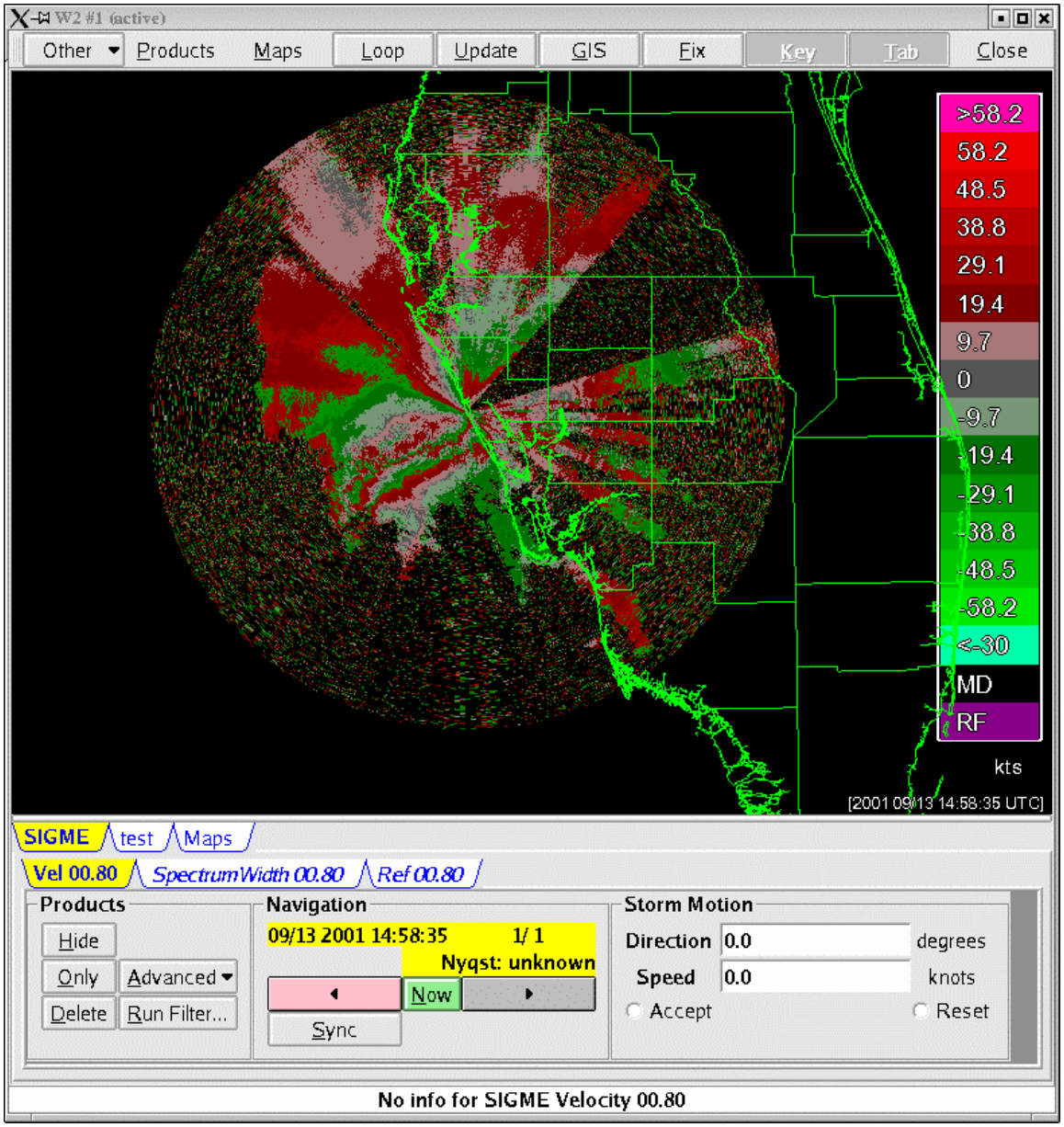

Figure 8: SMART-R velocity sweep

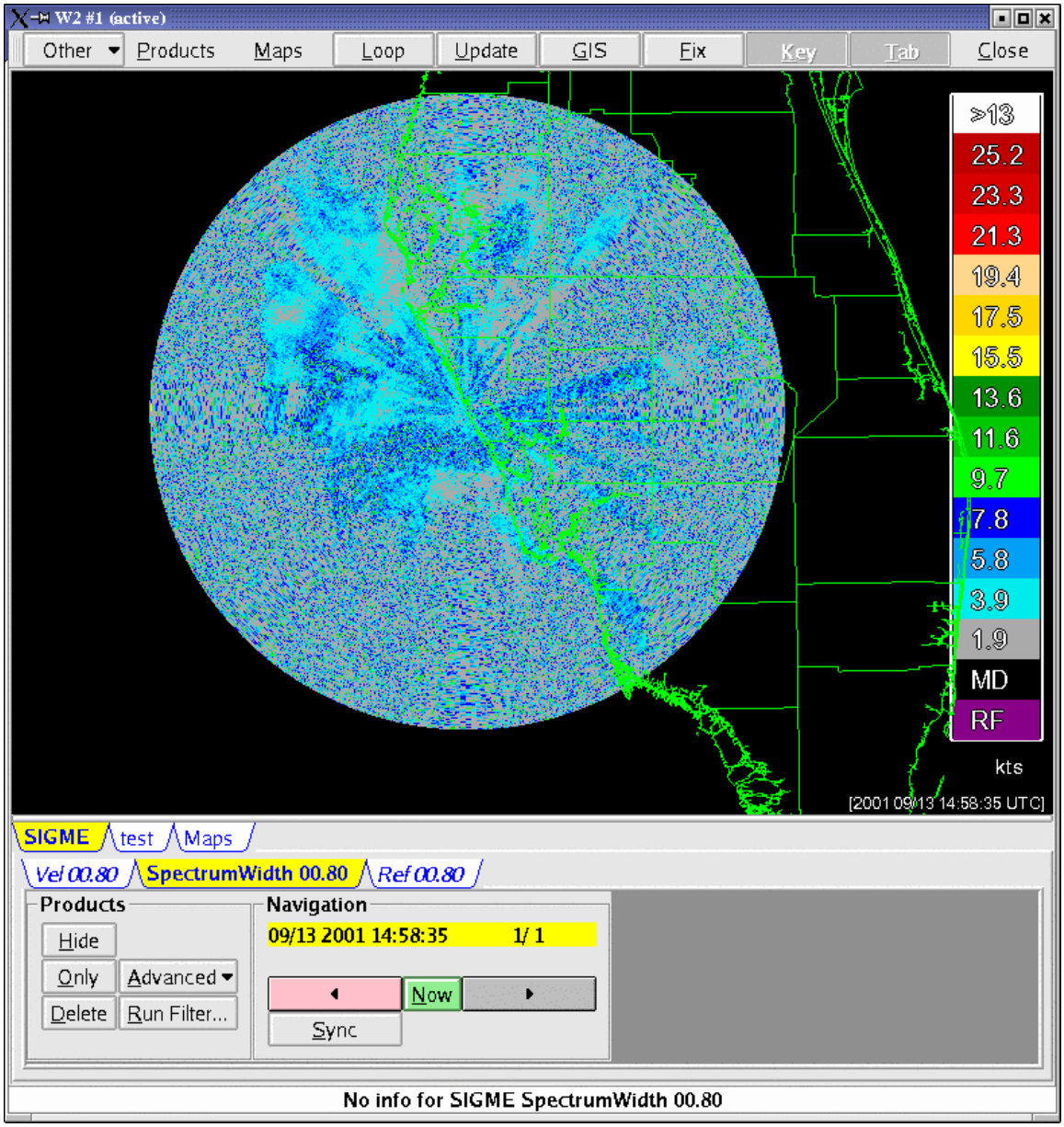

Figure 9: SMART-R spectrum width sweep

4. Enhancements to Clustering Algorithm

The K-Means clustering and motion estimation algorithm was enhanced to provide information about the clusters themselves. The clusters can be displayed, and information about the clusters are displayed as a table.

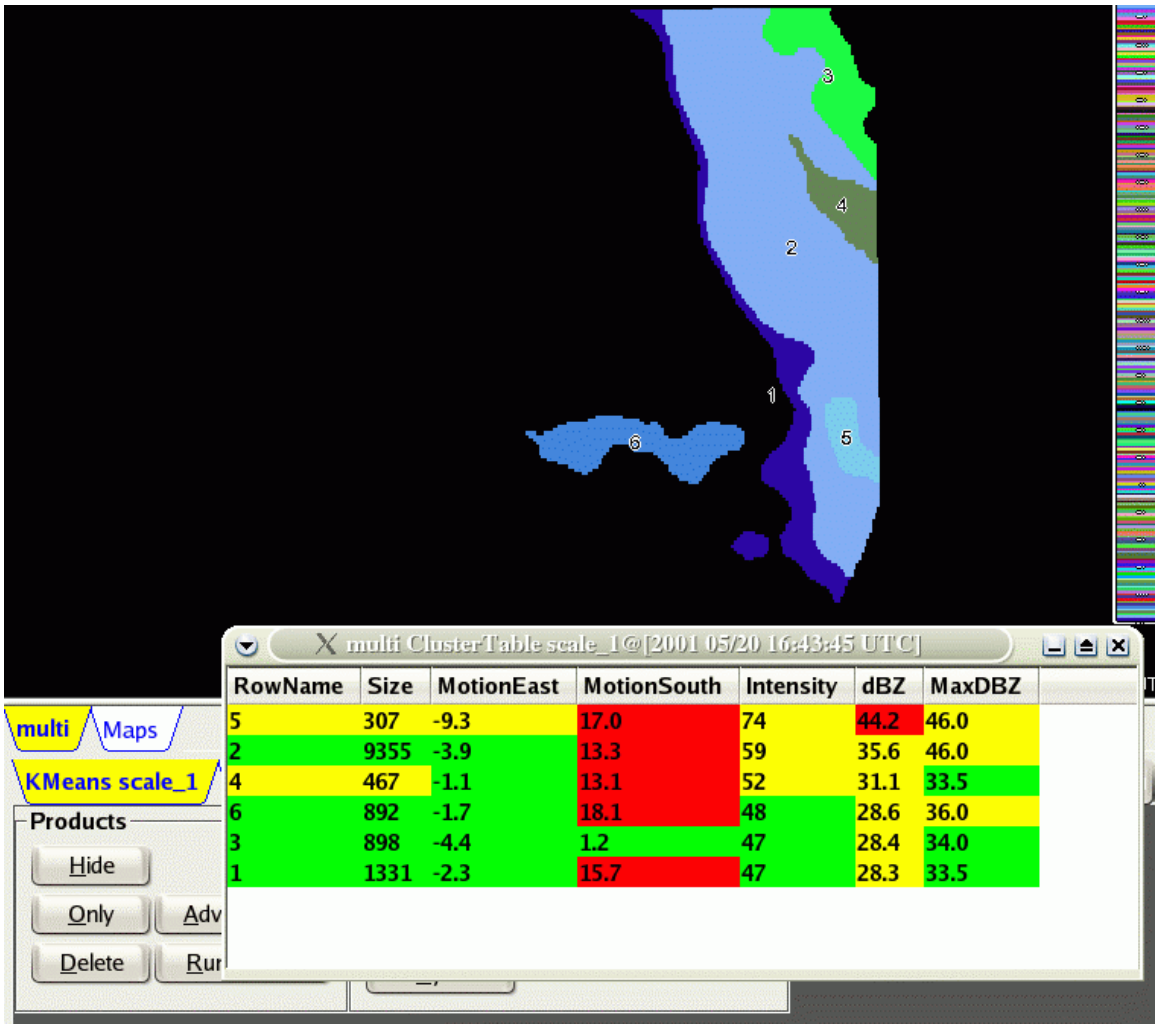

Figure 10: The K-Means clustering algorithm was enhanced to provide information about the clusters as a table.

Future enhancements include adding information such as VIL, Probability of Severe Hail, etc. and trends of these quantities.

5. Layer Average Product

At the request of the Space Flight meteorology group at NASA, we created a layer average product that they would like to use in determining flight paths. We also created reflectivity isotherms based on remapping radar data from multiple radars, and incorporating temperature information from the RUC2 model.

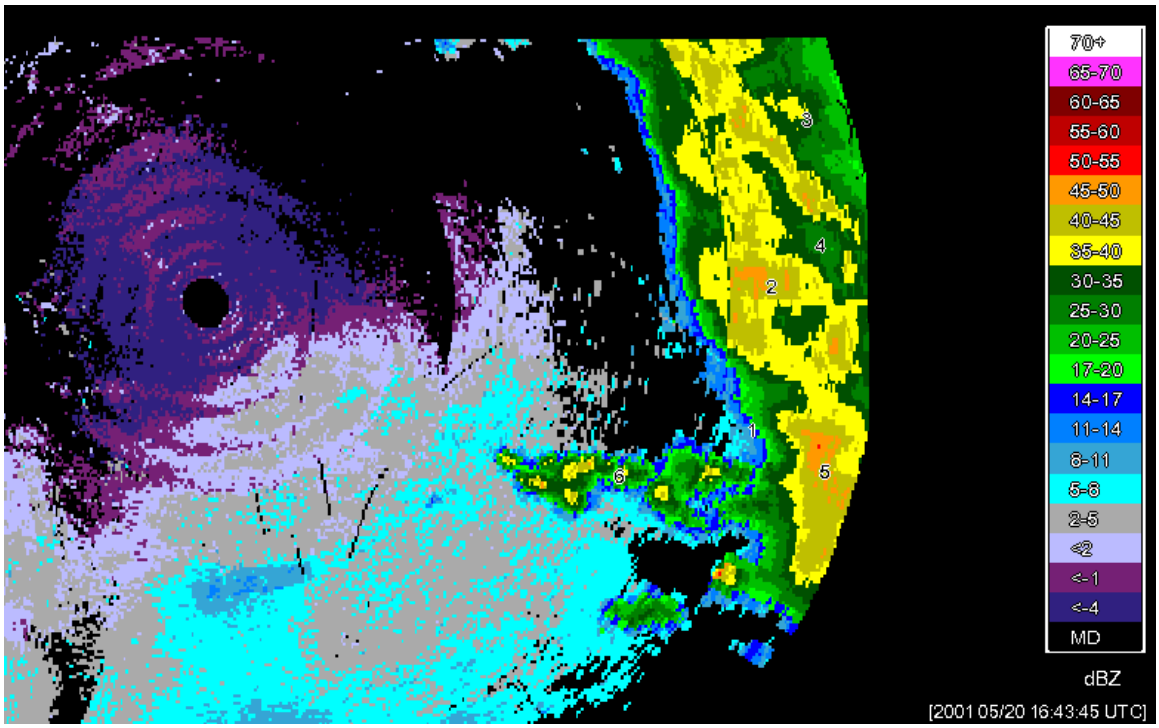

Figure 11: Reflectivity isotherm (at 0C) computed from multiple radars and the RUC model temperature field

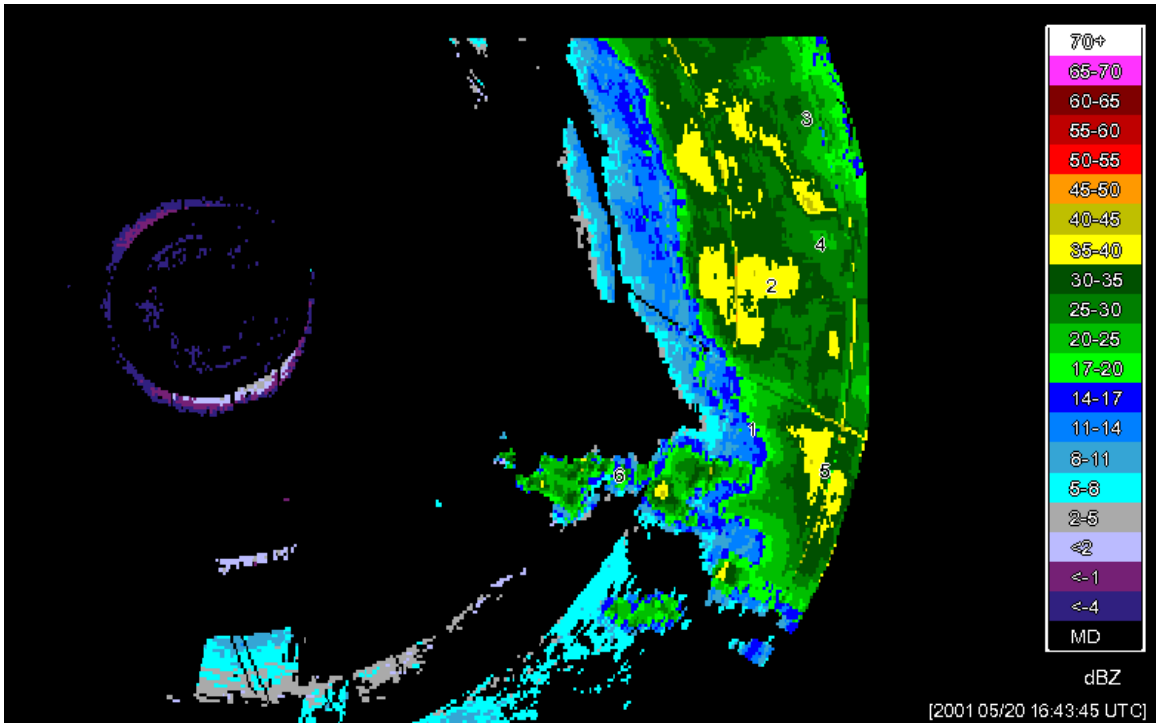

Figure 12: Reflectivity isotherm (at -20C) computed from multiple radars and RUC model temperature field

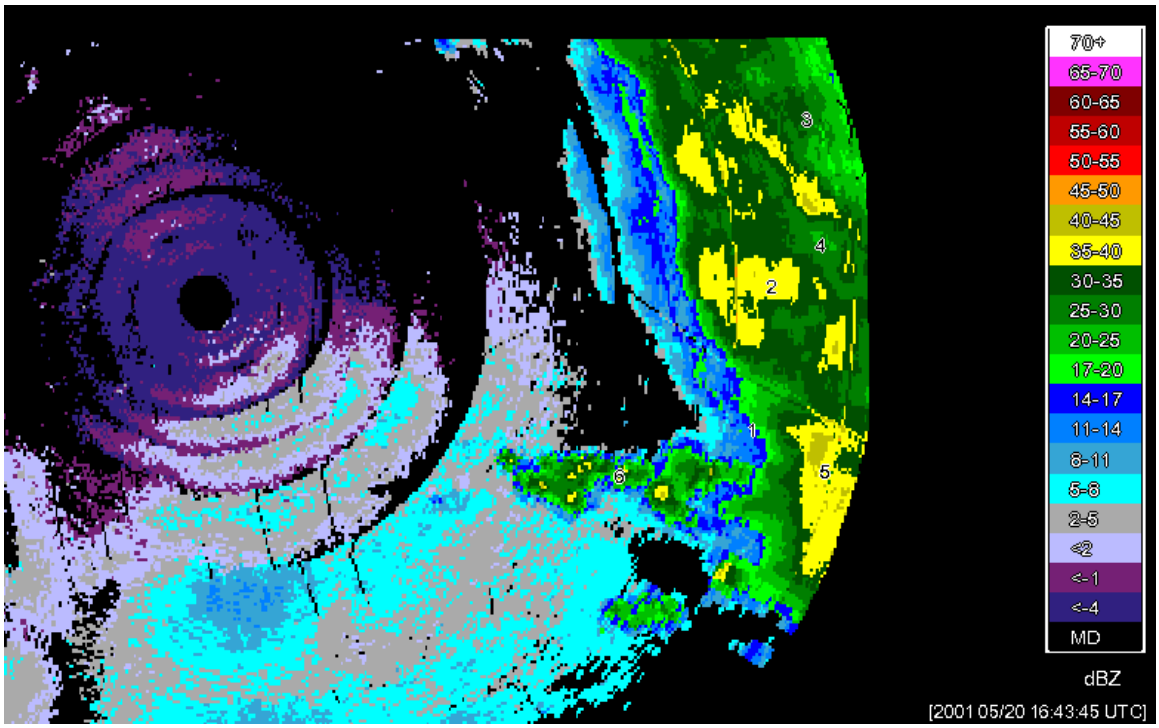

Figure 13: Layer average field computed by using the average radar reflectivity between the 0C and -20C levels. The radar reflectivity is obtained by fusing several NEXRAD radars, while the temperature field is obtained by ingesting the RUC2 model in real-time. The numbers indicate the clusters found by the K-Means clustering algorithm.

6. Other infrastructure and support work

- Several bugs were fixed in the Near Storm Environment program that caused the application to leak and sometimes stop processing new data.
- Continue work on developing 3-level iso-surfacing of radar data for 3D visualization.
- A new tool to generate the driver program for new algorithms was created. Now, creating the ingest for a brand new algorithm takes under 10 minutes.
- Added Nyquist information to polarimetric (KOUN) data, and assisted researchers in dealiasing the KOUN data.